Accepted Manuscript

Brain connectivity analysis from EEG signals using stable phase-synchronized states during face perception tasks

Wasifa Jamal, Saptarshi Das, Koushik Maharatna, Indranil Pan, Doga Kuyucu

PII: S0378-4371(15)00349-0
DOI: http://dx.doi.org/10.1016/j.physa.2015.03.087
Reference: PHYSA 16074

To appear in: *Physica A*

Received date: 6 June 2014
Revised date: 26 February 2015

Please cite this article as: W. Jamal, S. Das, K. Maharatna, I. Pan, D. Kuyucu, Brain connectivity analysis from EEG signals using stable phase-synchronized states during face perception tasks, *Physica A* (2015), http://dx.doi.org/10.1016/j.physa.2015.03.087

Brain Connectivity Analysis from EEG Signals Using Stable Phase-synchronized States during Face Perception Tasks

Wasifa Jamal[1], Saptarshi Das[1], Koushik Maharatna[1], Indranil Pan[2], and Doga Kuyucu[1]

[1] *School of Electronics and Computer Science, University of Southampton, Southampton SO17 1BJ, United Kingdom.*

[2] *Department of Earth Science and Engineering, Imperial College London, Exhibition Road, London SW7 2AZ, United Kingdom.*

Authors' Emails:

wj4g08@ecs.soton.ac.uk (W. Jamal*)

sd2a11@ecs.soton.ac.uk, s.das@soton.ac.uk (S. Das)

km3@ecs.soton.ac.uk (K. Maharatna)

i.pan11@imperial.ac.uk (I. Pan)

dk2g09@ecs.soton.ac.uk (D. Kuyucu)

Corresponding author's phone number: +44(0)7508408746

Acknowledgement

The work presented in this paper was supported by FP7 EU funded MICHELANGELO project, Grant Agreement #288241. Website: www.michelangelo-project.eu/.

Abstract:

Degree of phase synchronization between different Electroencephalogram (EEG) channels is known to be the manifestation of the underlying mechanism of information coupling between different brain regions. In this paper, we apply a continuous wavelet transform (CWT) based analysis technique on EEG data, captured during face perception tasks, to explore the temporal evolution of phase synchronization, from the onset of a stimulus. Our explorations show that there exists a small set (typically 3 – 5) of unique synchronized patterns or *synchrostates*, each of which are stable of the order of milliseconds. Particularly, in the beta (β) band, which has been reported to be associated with visual processing task, the number of such stable states has been found to be three consistently. During processing of the stimulus, the switching between these states occurs abruptly but the switching characteristic follows a well-behaved and repeatable sequence. This is observed in a single subject analysis as well as a multiple-subject group-analysis in adults during face perception. We also show that although these patterns remain topographically similar for the general category of face perception task, the sequence of their occurrence and their temporal stability varies markedly between different face perception scenarios (stimuli) indicating towards different dynamical characteristics for information processing, which is stimulus-specific in nature. Subsequently, we translated these stable states into brain complex networks and derived some informative network measures for characterizing the degree of segregated processing and information integration in those synchrostates, leading to a new methodology for characterizing information processing in human brain. The proposed methodology of modelling the functional brain connectivity through these synchrostates may be viewed as a new way of quantitative characterization of the cognitive ability of the subject, stimuli and information integration/segregation capability.

Keywords—*brain connectivity; complex networks; Continuous Wavelet Transform (CWT); Electroencephalogram (EEG); k-means clustering; phase synchronization; synchrostate*

1. Introduction

The brain has areas of specialized neurons which are responsible for distinct functions. These assemblies influence each other through excitatory and inhibitory synaptic connections [1]. Ensembles of segregated cortical areas of the brain form a big coherent organization which dynamically interacts to steer the brain into specific cognitive states. The temporal evolution of these synchronized cortical areas is instrumental in understanding how the human brain performs certain tasks given a particular stimulus.

Functional brain connectivity is defined as the time based temporal correlations between distributed neuronal units or the synchronization of activation of brain areas when performing a particular cognitive task [2]. It is defined to be highly time dependent and changes on the scale of milliseconds [3]. Tracing time dependent functional connections will allow us to quantify the quality and stability of connections made in a stimulus specific way, therefore paving the way towards understanding the neurobiological disorders of the brain

[4]. Research has established phase synchronization as a key feature for communication between the brain regions [5][6][7], serving as the manifestation of underpinning mechanism of information exchange in brain during cognition. The main goal is to explore the temporal stability of phase-synchronization and to translate them into functional connectivity network giving an insight into how the brain interacts during a task. This will enable one to evaluate the possible existence of stimulus-specific information integration or processing capability.

The high temporal resolution of non-invasive Electroencephalogram and Magnetoencephalogram (MEG) has been widely used as the key tool for understanding such synchronization phenomena. The frequency domain study of phase synchronization is led by the assumption that if two points (i.e. two EEG electrode sites) are maintaining constant phase relationship over time, they can be considered as functionally synchronized or connected [8]. Therefore computation of phase coherence is fundamental in this approach and serves as the key biological mechanism for communication between different brain regions.

In the conventional EEG analysis, coherence is used to model synchronization [9][10][11] over the individual EEG bands. This is done by first taking Fourier transform of the time-series of each of the EEG channels and then computing pair-wise coherence between the electrodes. However, such approach mixes the effect of phase and amplitude when computing the inter-relation between a pair of EEG signals [12]. Studying phase synchrony independently is vital as phase interactions are independent of the neural firing rates in different regions providing an independent dimension to the study of neural information processing [1][8]. In addition to that, being based on Fourier transform, the conventional approaches do not preserve the temporal information of phase synchronization which is essential in studying the transient dynamics of information flow from the onset of a stimulus. Other coherence measures like mean phase coherence [13][14] computes the synchronization components by averaging over the entire time window resulting into an average synchronization measure. Multivariate approach based on directed transfer function (DTF) and partial directed coherence (PDC) proposed in [15] although estimates time-varying cortical connectivity, they do not compute the phase coupling which is a direct measure of information transfer between different brain regions. Apart from these, different measures of phase synchronization have been illustrated in [5] but again none of them preserve the temporal information about the evolution of phase synchronization. On the other hand, methods based on Hilbert and wavelet transform [16][17] allow extraction of phase information from a non-stationary signal like EEG and MEG and inherently preserve the time information as well as frequency information [18]. Subsequently they have been successfully applied to study the stability of synchronization in different neuronal processing scenarios e.g. seizure [19], sleep [20], schizophrenia [21], visual task [22] on EEG and MEG data. In Quyen *et al.* [23] wavelet based time-frequency domain phase locking estimation of EEG signals is introduced. In Mutlu *et al.* [24] and Fallani *et al.* [25], time varying brain connectivity analyses have also been explored considering the whole time course, using measures like phase locking value (PLV) and PDC for completing a specific cognitive task.

In this paper, we exploit the time-frequency preservation property of wavelet transform for studying the temporal dynamics or evolution of synchronization amongst different areas of the brain. Compared to the contemporary approaches, we here subdivided the time course by associating them with a finite number of phase-synchronized states (using clustering) to find out how their switching sequence describes the execution of the face-perception task involving different types of stimuli. Our aim is to propose a generic method to characterize dynamic brain connectivity associated with the quasi-stable phase synchronized patterns. This may in turn lay the foundation of a methodology that will allow one to reliably diagnose or characterize different atypical neuro-pathological conditions more accurately.

We have used CWT with complex Morlet wavelet as the basis function for analyzing the transient dynamics of phase synchronization for a face perception task as a tool for our exploration. EEG data from the Statistical Parametric Mapping (SPM) database [26] has been used for this purpose. Two sets of analysis have been done – normal face and a scrambled face perception respectively. Over the last decade face processing and recognition have been studied in great detail. The face processing system of human is extremely fine and has the capacity to recognize and discriminate between faces and different facial expressions and involves unique functional properties that do not exist in the recognition of other visual stimuli [27], [28]. Face-evoked EEG modulations are hence a good modality to study the functional properties in the human brain. Face stimuli is known for eliciting strong event related potentials (ERPs) due to their psychological salience [29]. Using face stimuli may lead to strong and relatively stable responses across individuals [30]. Face ERPs have been shown to give very promising results in visual stimuli-driven brain computer interface (BCI) applications [29], [30] as well. The present study shows that there exist a small set of distinct and discrete phase synchronization patterns or '*states*' over the scalp. Each of these discrete states are stable of the order of milliseconds and then abruptly switch to another state. The inter-state switching characteristic follows a well-behaved temporal sequence from the onset of the stimulus. For convenience we term each of these states as *synchrostate*. The observation of synchrostates is similar to the result described in [31] where millisecond order stable potential distribution – termed *microstates* – were observed over the scalp. The main difference here is that synchrostates show the existence of similar type of phenomena in the phase domain which is directly informative about the information coupling mechanism following the fundamental notion of phase synchrony. Although the basic patterns of the synchrostate are similar for both the normal and scrambled face perception scenarios (both being part of a face perception task in general), the sequence of occurrence and stability period for each of these synchrostates differ markedly between these two cases which may imply different information integration processes.

Traditionally the EEG frequencies are subdivided into five bands: δ (0-4Hz), θ (4-8Hz), α (8-12Hz), β (12-30Hz) and γ (30Hz and above). The research conducted in Boiten *et al.* [32] established that different cognitive processes yield responses in different EEG bands indicating the association of a particular frequency band to a specific cognitive task. Previous research conducted in the domain of face perception has reported different responses in different frequency band while processing various emotional face expressions [33][34]. The β rhythms have been reported to be linked to cognitive processing, visual attention and perception related modulations [35][36]. The effect of synchrostate is more prominent in the β band which has already been reported to be related to the process of visual perception [35][36]. This is the category where our chosen task of face perception falls into, although similar effects are also visible in other EEG bands.

Subsequently we use a phase synchronization index to objectively measure the temporal stability of each of these synchrostates. Finally, a synchronization index is used for constructing weighted undirected connectivity graphs corresponding to each of these synchrostates and complex network analysis techniques are utilized to extract a set of metrics that enables one to quantitatively characterize the functional brain connectivity during the task. This method of tracing time dependent functional connections will allow us to quantify the quality and stability of connections, in a stimulus specific way. It could also be useful in understanding the implications of different neuro-degenerative conditions as they exhibit different types of impairments in information integration.

To confirm that the proposed approach could be generalized for other datasets and to confirm the consistency of our findings in different experimental conditions without the loss of generality, we perform similar analysis on another dataset consisting of a group of 10

subjects with three different visual stimuli. The group analysis is conducted on the EEG obtained from multiple trials and multiple subjects with a comparatively lower number of electrodes and for three face stimuli i.e. famous, unfamiliar and scrambled face [37]. The successful application of this methodology to different data-sets and the consequent finding of synchrostates in these data-sets implies that the observation of synchrostates is consistent and this method can be applied to various datasets without loss of generality. There has also been a recent study on synchrostate analysis of a population average of 10 healthy and 10 autistic subjects, during face perception task [38] which shows consistent results and exhibit synchrostate phenomenon.

The rest of this paper is organized as follows. In Section 2 we discuss the adopted methods for phase synchrony analysis along with deriving brain connectivity measures from a complex network theoretic point of view. Section 3.1-3.4 presents the simulation experiment results for EEG signals acquired during normal and scrambled face perception task for a single subject. The brain connectivity analyses and objective measures for evaluating the information integration capability of brain for these two kinds of stimuli have been presented in Section 3.5. Validation of the proposed method on a group of 10 subjects during face perception task is reported in Section 3.6. The paper ends with the discussions and conclusions in Section 4 and 5 respectively, followed by the references.

2. Theoretical formulation

In this section, we discuss three particular issues that are fundamental for developing an integrated methodology for analyzing the temporal evolution of brain functional connectivity from the onset of a stimulus using EEG time-series data. These issues are: 1) the definition of an objective measure for capturing the effect of time-varying phase synchronization amongst the EEG electrodes, 2) clustering of characteristic phase difference patterns and formulating an index as a measure of their temporal stability, and 3) translating those unique clusters into a complex brain network using graph theoretical approaches and from those deriving quantitative measures for the brain's ability for information exchange. In the following subsections these three issues are discussed in detail.

2.1. CWT based phase synchronization measure in EEG signals

For the estimation of phase synchronization between two signals the first step is to compute the instantaneous phase difference between them and then to estimate the degree of phase locking over a period of time [12]. Continuous complex wavelet transform applied on two given signals $x(t)$ and $y(t)$ yields two complex time series $W_x(a,t)$ and $W_y(a,t)$ respectively and their instantaneous phase difference at time t in wavelet scale a can be computed as (1) with $\varphi_x(a,t)$ and $\varphi_y(a,t)$ being the arguments of the complex term of the $W_x(a,t)$ and $W_y(a,t)$ respectively [39].

$$\Delta\varphi_{xy}(a,t) = \left|\varphi_x(a,t) - \varphi_y(a,t)\right| \tag{1}$$

The instantaneous phase matrix is given by the argument of the continuous complex Morlet wavelet transform of the signals on each EEG channel and subtracting it from the other electrodes. The complex Morlet wavelet basis function used here is given by (2).

$$\Psi_M(t) = \frac{1}{\sqrt{\pi F_b}} e^{2j\pi F_c t} e^{-\left(t^2/F_b\right)} \tag{2}$$

where, $\{F_b, F_c\}$ denote the bandwidth parameter and the center frequency respectively. For the present simulation, we used $F_b = 1, F_c = 1.5$.

As the instantaneous phase difference is a function of wavelet scale a (and hence frequency) and time t, equation (1) can be utilized to formulate a series of time- and frequency-specific phase difference matrices over several wavelet scales to study a broader frequency range. For a more comprehensive analysis we converted the resultant complex series which is a function of scale and time to a function of frequency and time using the following relation (3).

$$F_a = F_c / (a \cdot \Delta) \tag{3}$$

where, $\{a, \Delta, F_a\}$ represent the scale, sampling period and the pseudo-frequency respectively.

Since each of the characteristic EEG bands is composed of a range of frequencies, in our analysis, we computed the phase difference over all the frequencies belonging to a specific EEG band for a pair of electrodes (x, y) and then finally calculated an average of them to formulate a frequency band specific $\Delta\varphi^B_{x,y}(t)$ which is given in (4).

$$\Delta\varphi^B_{x,y}(t) = \frac{1}{a_2 - a_1} \sum_{a=a_1}^{a_2} \Delta\varphi_{x,y}(a,t) \quad \forall x, y \in \{1, 2, \cdots, N\}, B \in \{\theta, \alpha, \beta, \gamma\} \tag{4}$$

where, a_2 and a_1 are the scales corresponding to the upper and lower bounds of the frequency band B respectively and N is an integer representing the number of EEG channels.

The time varying band averaged phase differences calculated using (4) can now be clustered into groups employing a certain class of pattern recognition algorithms. In order to explore possible existence of characteristic patterns of phase synchronization that are stable for finite time, we used the *k*-means clustering method which is a classical unsupervised-learning pattern recognition technique. It uses the squared Euclidean distance to measure dissimilarity between data vectors. Given a dataset χ, assuming that the number of underlying clusters is known, *k*-means iteratively minimizes the cost function $J(\theta, U)$ as shown in (5).

$$J(\theta, U) = \sum_{i=1}^{P} \sum_{j=1}^{m} u_{ij} \left\| X_i - \theta_j \right\|^2 \tag{5}$$

where, $\theta = \begin{bmatrix} \theta_{T_1} & \cdots & \theta_{T_m} \end{bmatrix}^T$, $\|\cdot\|$ is the Euclidean distance, θ_j is mean vectors of the j^{th} cluster and $u_{ij} = 1$, if the i^{th} data-point X_i lies closest to θ_j; 0 otherwise [40]. Here, $\chi = \{X_i\}, i \in [1, \cdots, P]$ is the dataset of all pairwise EEG instantaneous phase differences in a particular band *B*, as a function of time calculated using (4). We clustered the dataset χ along time, for a chosen frequency band, to find out unique phase synchronized patterns.

Initially, arbitrary *k* centroids are defined and the data vectors X_i are designated to a class, depending on how near they are to the centroids. The parameters are updated and θ_j are recalculated from the clusters defined in the previous step and subsequently the data

vectors are reassigned to these new recalculated centroids. The algorithm iterates over this loop until the data vectors from χ form compact clusters i.e. there is no change in θ_j between two successive iterations and J is minimized [41]. The optimization algorithm runs the *k*-means clustering n times for each m (number of clusters) in a defined range $[m_{\min}, m_{\max}]$ for the dataset χ to find the optimal number of underlying clusters. For every n runs (set to 10 for the present simulations), the minimum value of J_m is stored. If the plot of J_m against m indicates a characteristic 'knee', it signifies the number of clusters that is likely to underlie the dataset χ [40]. Note that it is possible to have multiple 'knees' in such plots as changing *m* may imply breaking of compact large clusters into smaller less compact clusters and subsequently showing sharp rise in J_m for certain *m*. In such cases, as conventionally followed in machine learning, the earliest and the most prominent knee should be considered as the characteristic knee, as it explains the underlying dataset with minimum complexity. The main information lies in the fact how many compact clusters can be identified in the whole dataset and what are the average characteristics of the data-points associated with each cluster. Thus the absolute value of J_m in the plot of J_m against *m* is not important but the value of *m* at which J_m attains minimum value (the significant knee) is the important parameter indicating the number of underlying clusters.

It is well known that the phase and hence the phase difference data is circular in nature (circular data) therefore standard Euclidean distance based clustering should not be directly applied on such datasets [42]. In order to circumvent this problem, we first ensured that the phase of CWT based complex time-frequency decomposition is always bounded within $\varphi_x \in [-\pi, \pi], x \in [1, \cdots, N]$. Next the phase difference data for all electrode pairs were normalized using the minimum and maximum values of the phase difference $\Delta\varphi_{xy}^{\max} = 2\pi$ and $\Delta\varphi_{xy}^{\min} = 0$, so that the transformed data lies within $\Delta\varphi_{xy}^{normalized} \in [0,1]$. This transformed phase difference data was fed to the clustering algorithm described in (5).

Once such possible unique clusters are identified, their temporal stability needs to be analysed since the clustering technique only identifies possible unique stable phase difference patterns but it does not capture the length of time for which each of them are stable. Quantitatively, this can be described by the synchronization index $\Gamma_{xy}(B)$ which is an inverse circular statistical analogue of variance given in (6) [39].

$$\Gamma_{xy}(B) = \frac{1}{P_s}\sqrt{\left[\sum_t \cos\left(\Delta\varphi_{x,y}^{B}(t)\right)\right]^2 + \left[\sum_t \sin\left(\Delta\varphi_{x,y}^{B}(t)\right)\right]^2} \tag{6}$$

Here, P_s is the number of data-points in the clustered time series with $P_s < P$ or it can be viewed as the time points associated with a single state (*s*) and $\Gamma_{xy}(B) \in [0,1]$. A high value of $\Gamma_{xy}(B)$ indicates that the phase difference between the two signals at a given frequency band B has low variation over time and therefore can be considered in synchrony. This in essence quantifies the average temporal stability of the clustered phase synchronization states in that band. In contrast to the coherence based measures [5] this index is capable of capturing the band-specific temporal behaviour of the synchronization phenomena. Once the values of $\Gamma_{x,y}$ are computed for each of the channel pairs (x, y) they can be plotted for all

the electrodes resulting in a global synchronization matrix which is symmetric and square in nature describing the temporal stability of phase synchronization in the entire EEG space.

2.2. Complex network measures of brain connectivity

After the global synchronization matrix describing the stability of each of the clusters is formed it can be translated into a complex network that may shed light on the temporal evolution of phase synchrony amongst different brain regions and hence describe the nature of associated information coupling. Similar to the other connectivity networks in nature, brain connectivity can be analyzed with the graph theoretic approach by considering the EEG electrodes as nodes and the $\Gamma_{x,y}$ values between them expressed as weighted edges signifying the connection strength between the $(x,y)^{th}$ node. The usefulness of complex network analysis was demonstrated in the study of anatomical as well as functional brain networks [43]. Network measures have been used to quantify the brain connectivity [44][45] and have been useful to draw network topology comparisons between healthy subjects and patients with neurological injury or disorder [46][47][48]. The topological properties and intrinsic meaning of the networks thus created can then be studied by interpreting the appropriate network measures. Two specific types of generic measures that are most relevant in understanding the brain's capability for information processing are segregation and integration. Owing to the inherent complex nature of the human brain the existence of functional integration and specialization can quantitatively determined by defining a measure of complexity [49].

Modularity (Q^w) of a network quantifies the network segregation measuring the extent to which a network can be subdivided into a group of nodes with small number of between group links (edges) and large number of within group links [50] and is expressed as (7).

$$Q^w = \frac{1}{l^w}\sum_{x,y\in N}\left[w_{xy} - \frac{k_x^w k_y^w}{l^w}\right]\delta_{m_x,m_y} \tag{7}$$

where, w_{xy} is the connection weights, $k_x^w = \sum_{y\in N} w_{xy}$ is the weighted degree, $l^w = \sum_{x,y\in N} w_{xy}$ is the sum of all weights in the network. Also, $\delta_{m_x,m_y} = 1$ if $m_x = m_y$, and 0 otherwise (m_x is the module containing node x). Here, the superscript w indicates the weighted nature of the graphs, as adopted in the present analyses, whereas binary and directed versions are also possible.

Transitivity (T^w) which is the ratio of the triangle to triplets of the network is also a measure of segregation in complex network analysis and is a normalized variant of clustering coefficient [51] which is expressed as (8).

$$T^w = \frac{\sum_{x\in N} 2t_x^w}{\sum_{x\in N} k_x\left(k_x - 1\right)} \tag{8}$$

where, $t_x^w = \frac{1}{2}\sum_{y,h\in N}\left(w_{xy}w_{xh}w_{yh}\right)^{1/3}$ is the weighted geometric mean of the triangles around x.

Characteristic path length (L^w) and global efficiency (E^w) are common measures of integration which captures the capacity of global interaction in a network and may represent the ease of network–wide communication [3]. The degree of integration in a network is based

on the efficiency of global communication and on the ability to integrate distributed information from specialized regions of the brain [52]. Characteristic path length, given in (9) is the average of the shortest path length between a node and all other nodes [53]. It is the global mean of the distance matrix. On the other hand, the global efficiency, given in (10) is computed by averaging the inverse of the distance matrix. Therefore a fully connected network has maximum global efficiency [3].

$$L^w = \frac{1}{\widetilde{N}} \sum_{x \in N} \frac{\sum_{y \in N, y \neq x} d_{xy}^w}{\widetilde{N} - 1} \tag{9}$$

$$E^w = \frac{1}{\widetilde{N}} \sum_{x \in N} \frac{\sum_{y \in N, y \neq x} \left(d_{xy}^w \right)^{-1}}{\widetilde{N} - 1} \tag{10}$$

where, d_{xy}^w is the shortest weighted path length between x and y.

The widely used graph theoretic measures that measure the ease of global communication in networks use the concept of paths and essentially estimate the average length of the shortest communication paths between nodes [52][54]. The two important measures i.e. radius and diameter of any complex network can be derived from its eccentricity (e_x^w) which refers to the maximum value of each row of the Hadamard (dot) product of d_{xy}^w. Radius (r) and the diameter (D) are the minimum and the maximum values of eccentricity respectively and are mathematically expressed as (11).

$$e_x^w = \max \left(d_{xy}^w \circ d_{xy}^w \right), r^w = \min \left(e_x^w \right), D^w = \max \left(e_x^w \right) \tag{11}$$

Quantitative measures of the above mentioned metrics therefore are expected to characterize the ability of the brain network for information processing in terms of specialized processing (segregation) within local regions and global integration. In the above mentioned network parameters (7)-(11), N is the set of all nodes in the network and $\widetilde{N}$ is the number of nodes.

The neurobiological context and significance of modularity and transitivity is that they quantitatively describe the highly segregated communities with information passing within them [3][55]. Nodes belonging to a cluster or module share significant information with each other. On the contrary, units belonging to different clusters remain segregated from each other with little interaction between them. The segregated modules specialize in their own task and function, however executive functions (integrative processes), benefit from high global efficiency and require continuous and efficient information transfer across different regions as they form a complex integrative network [56]. However, it is to be noted that measurement of phase synchrony represents only the information coupling strengths amongst different brain regions rather than giving a direction of information flow. Therefore, in this work we have restricted ourselves to the analysis of weighted undirected brain networks only.

3. Data analysis workflow during face perception

The simulations are all run on EEG data collected during face-perception tasks. The first exploration was conducted on a single subject multiple trial dataset. After the phase relations were investigated, an extensive set of simulations were run on the same data to investigate the consistency related to the different grouping of EEG trails. Once the phase synchronized functional connectivity was derived from this data set, a detailed analysis was carried out on the graph theoretic brain connectivity measures. Once the method was

established, the same analysis was applied to EEG from 10 subjects with multiple trails. All EEG data was baseline corrected and epochs over 200μV threshold were rejected. Data was then band-pass filtered within 0.5-50 Hz using a 5^{th} order digital Butterworth filter to isolate the EEG bands of interest.

3.1. Analysis of single subject multiple trial EEG dataset

The simulations were carried out on the SPM multimodal face-evoked dataset [26]. This data was acquired from a single subject while the person was presented images of normal and scrambled faces. The stimulus dataset consisted of 86 normal and 86 scrambled face images. The EEG recording was done by randomly selecting stimuli from this set and presenting it to the subject, multiple times creating multiple trials for each type of stimuli. The data was sampled at 2048 Hz and was recorded on 128 EEG channels over several trials of which the first 100 trials were used for our analysis. Epochs were created from -200ms pre-stimulus to 600ms post-stimulus. In order to compensate for the variability of our results and to investigate its consistency over different trials we have divided the whole data set into two non-overlapping groups (2 blocks of 50 trials: trial 1-50 and trial 51-100) and taking all the trials (1 block of 100 trials: trial 1-100) as the third group. This is done from the point of view that the ensemble statistics or the pattern underlying the cross-electrode phase difference should be consistent over small subsets of multiple trials and the trials consisting of the entire dataset. For each of the runs, the instantaneous phase difference between all pairs of electrodes were computed following the procedure described in Section 2.1. The cross-electrode relative phase at a particular time instant is represented as a symmetric square matrix with zero diagonal elements as they represent the phase difference of an electrode to itself. These matrices were then averaged across the number of trials considered during that run. Observation of this resultant multi-channel phase data in a sequence of intervals of the order of milliseconds reveals the existence of discrete and distinctive patterns that are stable over finite number of time-frames. This is an interesting observation, as it is similar to the concept of microstates in [57] where the authors observed stable potential distribution maps over millisecond order time segments. Similarly, we observe that the phase difference maps remain stable for certain time interval of the order of milliseconds i.e. they are phase synchronized and then suddenly change to a new configuration that also remains stable for finite time. We define these temporally stable phase synchronized states as *synchrostates*. The temporal stability of such synchrostates may be indicative of the time, required for maintaining such a phase relationship between different regions of the brain in order to perform a certain task – in this case, a face perception task.

In order to determine these synchrostates optimally, we perform *k*-means clustering over the time series of all phase matrices, to associate similar patterns into a single class, following the method described in Section 2.1. Here, the hard clustering algorithm is applied with the assumption that the brain can be at only one state at a particular time instant. We transform each instantaneous phase difference matrix which is a function of time and frequency, into a vector and then apply *k*-means clustering algorithm on 400 time instances (samples).

We perform incremental *k*-means clustering over the time series of all phase matrices along time *t*, for a chosen frequency band (θ, α, β, γ), to find out the unique phase difference patterns. The *k*-means clustering finds out similar states (named as state 1, 2 and 3) using an unsupervised learning mechanism. The algorithm yields *k* centroids for each cluster or state and a vector of length *t*, with the corresponding state or cluster labels for each phase difference matrix, for every time instance, along which we clustered the data. All the data-

points within a cluster are considered to have a generalized characteristic of that of the mean of the cluster, even though they can slightly differ from each other, as they possess EEG temporal information of the order of milliseconds. The state labels are used to construct a transition plot to illustrate the transients of the synchrostates over the time of the EEG recording. This is simply done by plotting the time labels yielded by the clustering algorithm. The consecutive occurrences of same labels (i.e. similar phase synchronized patterns) have been interpreted as the prevalence of the same state. On the other hand, sudden changes in the cluster label (i.e. different phase-difference pattern) from previous clusters are considered as switching of the state.

3.2. Analysis for normal face

Figure 1 shows the results from all the three runs of the optimization routine for optimally clustering the synchrostates in the β band when applied on EEG data for normal face perception task. In this case, over all the runs the *k*-means clustering consistently results into three unique states as there exists a '*knee*' in the cost function (J_m) at $k = 3$.

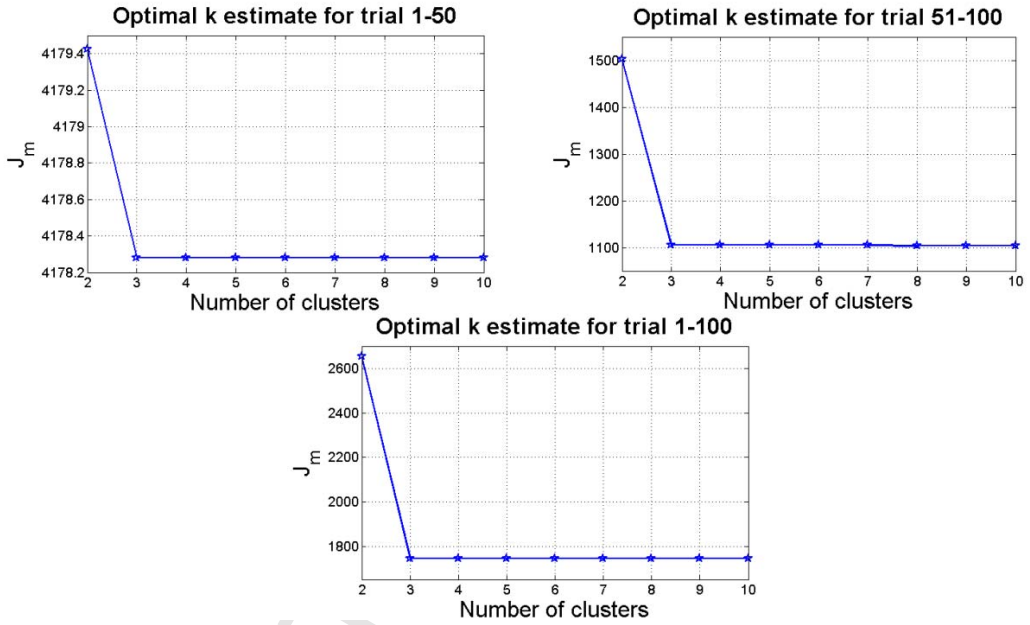

Figure 1: Determination of the optimum number of underlying clusters (*k*) for different group of EEG trials during normal face perception in the β band.

After obtaining three unique synchrostates, the cross-channel EEG phase differences are averaged for each electrode to get an average phase corresponding to that node. These are next used to generate a contour plot over a head-map by connecting nodes having the same average phase difference values. The topographical distributions or contour plots of each of these three synchrostates are shown in Figure 2. Note that the topographies should not be interpreted like standard quantitative EEG (qEEG) plots (which show the average spectral power over the scalp), as they are fundamentally different. Here, the plots show the gross phase difference between different electrodes over the scalp during the occurrence of the state. Such head-map topographies give a visual representation of the distribution of average phase differences between different regions of brain over the scalp. Higher numerical values (reddish hues) represent greater gross phase difference of the electrode with respect to all the other electrodes and low values (bluish hues) indicate that the electrode has relatively less phase difference relative to all other electrodes, in that configuration. It is interesting to note

that the topographical maps of synchrostates are consistent across different set of runs and are almost unique in our simulation. In Figure 2, there is some slight difference in the first state topography, especially in the fronto-central electrodes. This much of difference is expected due to variability of the trials, mood or mental condition of the subject, attention level, particular characteristics of the face stimulus and various other subconscious random processes going on within the brain during the data-recording. In most literature on EEG studies, there is evidence of such inter-trial variability [58][59]. Despite these incongruences, the main unifying theme among these plots is that almost similar phase synchronization phenomenon can be observed in these states.

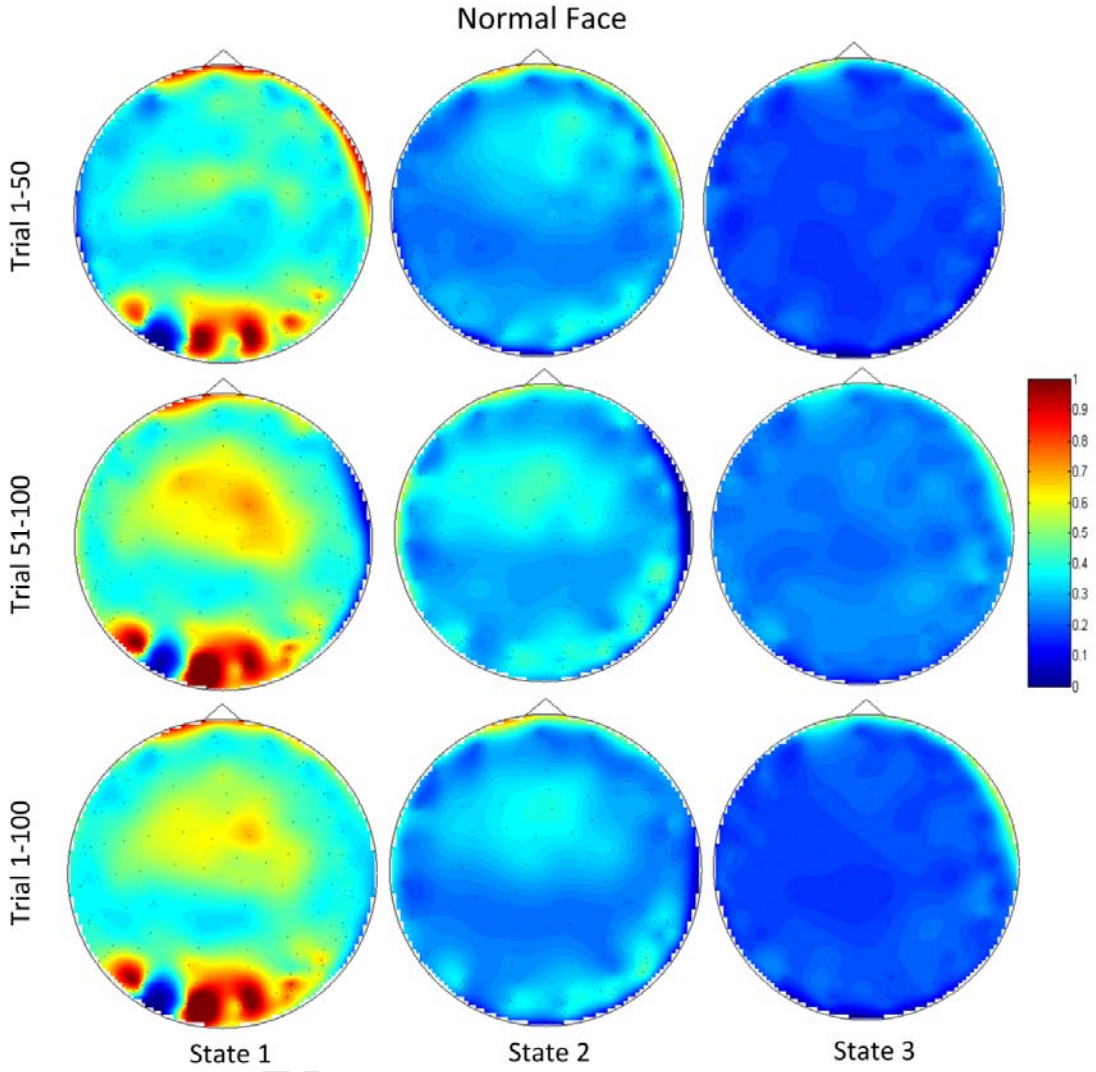

Figure 2: Clustered synchrostates for trials 1-50, 51-100 and 1-100 of normal face perception in the β band.

Also in the side edges of the head in Figure 2, concentration of large phase difference should not be confused with the presence of artifacts. This is because the synchrostates change at the time resolution of milliseconds (ms) and the artifacts generally occur in the time interval of seconds. Had there been any artifact in the EEG, all the states (state 1-3) would have been corrupted, in an almost similar way. Because artifacts could not appear in millisecond level time resolution, then disappear and again reappear within this small time window, they do not account for the observation of the synchrostates, as all states are following a switching sequence in a small window of time. Trials with recording over 200µV threshold were rejected and not considered in the analysis as artifacts. Eye artifacts are

generally concentrated in the forehead and are constrained mainly in the low frequency ranging from 1-5 Hz [60]. Muscle activity is reported to be maximal at frequencies higher than 30 Hz [61][62][63]. It is also well known that prominent broad-band signal power above 30 Hz can be attributed to micro-saccadic artifacts [64]. The plots in Figure 2 are the results in the β band (13-30 Hz) synchronization, so are likely to be minimally affected by eye or muscle artifacts.

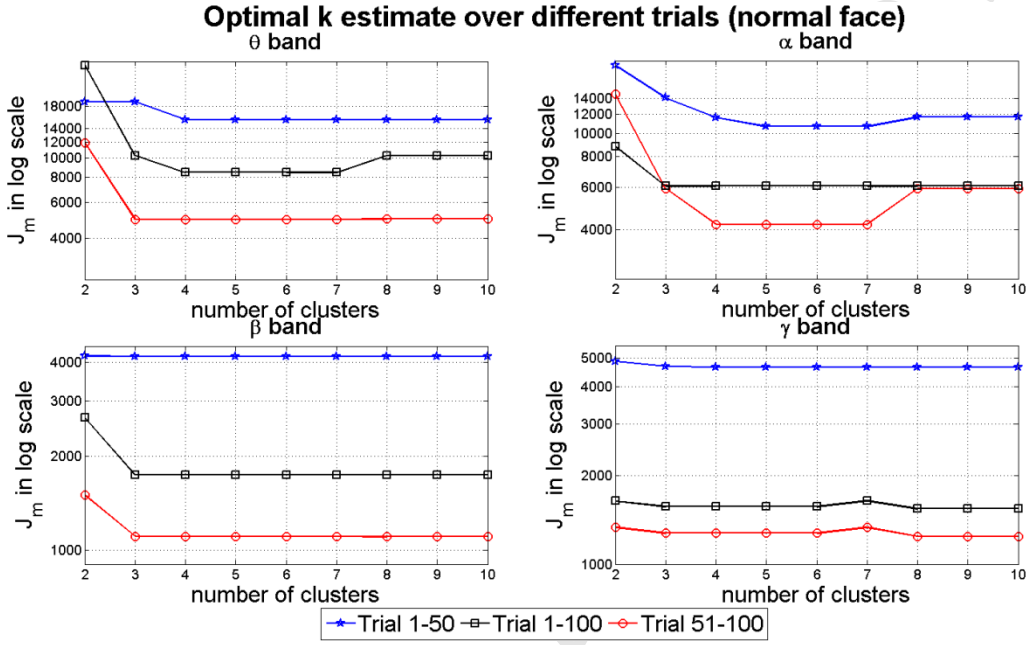

Figure 3: Cost functions for clustering in different EEG bands with increasing k during normal face perception.

Table 1: Number of Occurrence (time instants) for Three States in β Band with Normal Face Stimulus

EEG segments	State 1	State 2	State 3
trial 1-50	101	43	256
trial 51-100	105	31	264
trial 1-100	113	42	245
Mean	106.33	38.67	255

To explore the repeatability of the synchrostates for the present task, we computed the number of times each of these states occurs in the β band. The results, as shown in Table 1, confirm that the number of occurrence of each of the synchrostates is consistent over separate trial groups with little difference. The little variation observed could be attributed to the fact that even during a focused task, there could be multiple cognitive processes that run in the background. These may not be directly related to that specific task but may influence the phase relationship between different brain regions in an indirect way.

We applied the same technique for extracting the synchrostates in the θ, α and γ bands and the cost function results are shown in Figure 3. We found that in θ and α band, the optimal number of synchrostates varies between separate trials but within a small range (approximately 3-5) whereas, for γ band the optimal number of synchrostates is obtained at $k=3$ consistently. This small variation of optimal number of synchrostates in the α and θ

bands may once again be attributed to the fact that they represent different background cognitive processes, executed during the cognitive task which are not directly related to the present task and therefore may vary between the trials.

3.3. Analysis for scrambled face

A similar analysis has been carried out for the scrambled face case. Figure 4 shows the optimal k for the scrambled face run in the β band which is once again obtained at $k = 3$. We also plotted the normalized average phase difference head plots similar to those for normal face perception in β band to get a better idea of the topographical structures of the synchrostates which are shown in Figure 5. Interestingly, the maps appear very similar to the plots resulting from the normal face stimuli showing that the actual phase topographies remain same for both of the tasks. In one sense this is expected as both of the tasks fall into the generic category of visual perception. However, the optimal number of synchrostates in the other EEG bands (θ, α, γ) once again varies from 3 to 5 in this case as shown in Figure 6, as it was during a normal face perception task. Once again this phenomenon is attributed to the existence of background cognitive processes, independent of the present task and inter-trial variability.

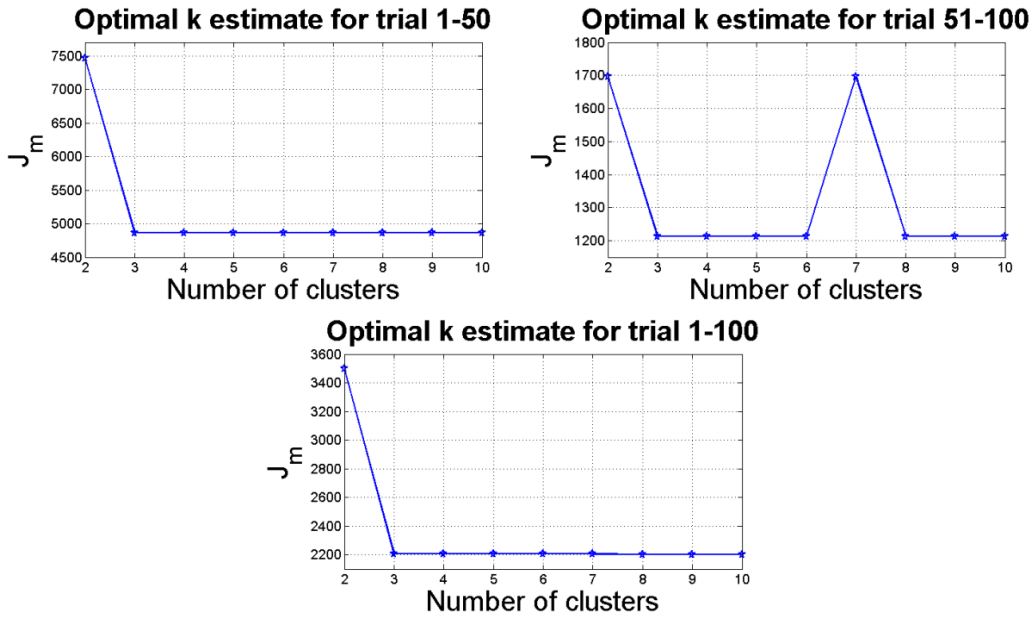

Figure 4: Determination of the optimum number of underlying clusters (k) for different group of EEG trials during scrambled face perception in the β band.

The existence of consistent number of synchrostates in β band for both the cases conforms to the theory that β rhythm is more related to visual perception tasks [35][36] and therefore one may expect dominant and stable information exchange patterns in the β band. On the other hand, the very small variability of the number of optimal synchrostates in the other EEG bands (3 – 5 in both the cases) also indicates towards consistency of the existence of synchrostates in these bands.

Table 2 shows the number of times each state has occurred for each run during the presentation of scrambled face stimulus in the β band. The important point to note is that in this case although the topographic maps of the synchrostates are similar to those of the normal face perception stimulus, the number of occurrence of each of them is markedly different. State 3 although shows a similar number of occurrence to that of the normal face perception,

the number of occurrence of state 1 and state 2 differ significantly between the two cases. A close observation reveals that the state 1 occurs more frequently during normal face processing whereas state 2 occurs more often during the scrambled face processing indicating towards different types of processing which is dependent on the type of stimulus.

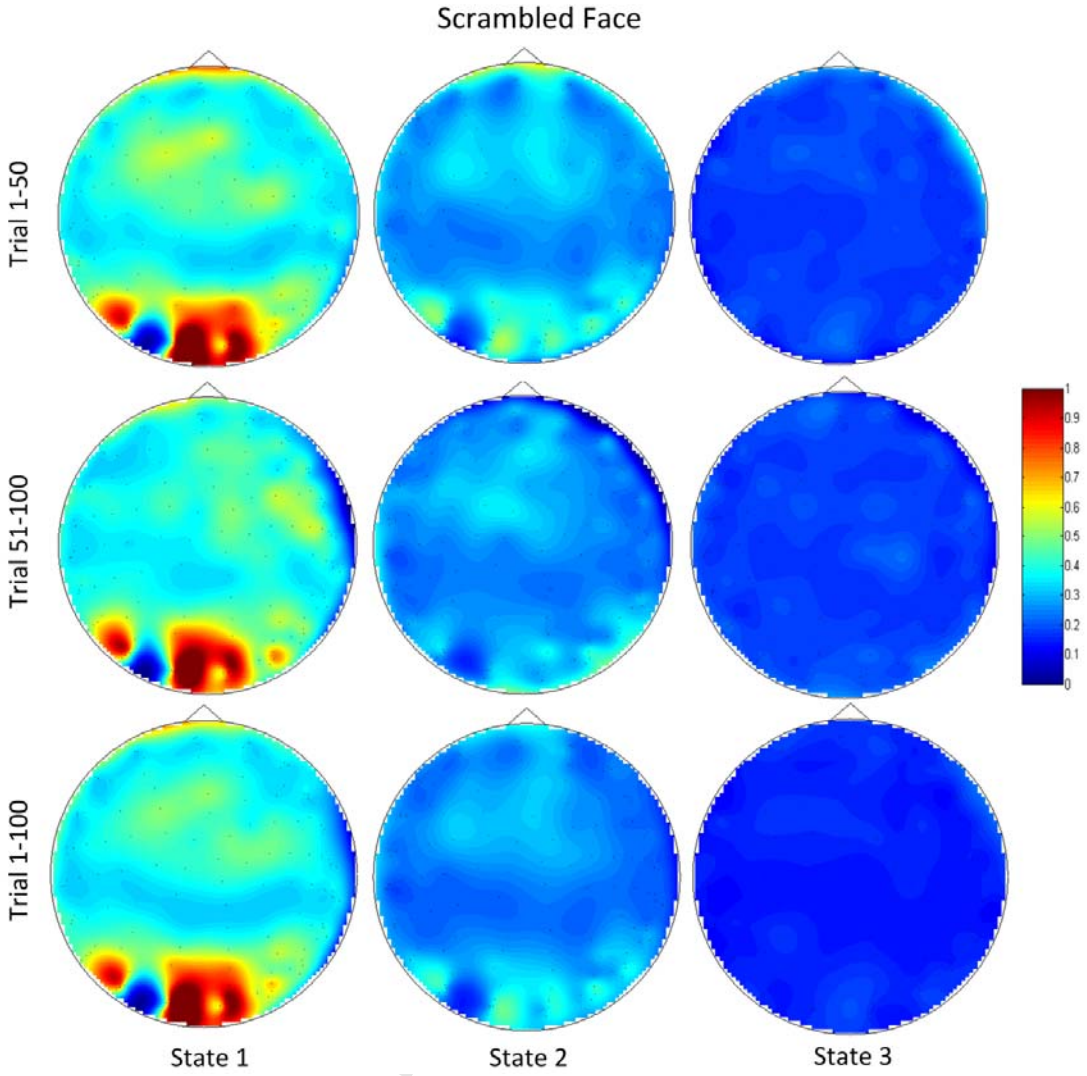

Figure 5: Clustered synchrostates for trials 1-50, 51-100, 1-100 of scrambled face perception in the β band.

In order to distinguish between the time-course of each synchrostate specific to a stimulus that may be indicative to the processing time required for a task, we plotted their switching time-course over 400 samples (approximately 195 ms) after the onset of the stimulus for both normal and scrambled face as shown in Figure 7. As can be seen from Figure 7, the switching time-course of the synchrostates for different trials for each of the considered cases follow a consistent pattern, whereas they are markedly different between the normal and scrambled face perception, indicating toward the stimulus-specific nature of it.

In order to generate the transition plots in Figure 7 over different group of trials, the EEGs in different trials are averaged and then the synchrostate analysis was run on each of the average EEG signals. This yields a single transition plot for a group of trials. Each subplot in Figure 7 shows that the switching transition between the 3 states obtained from the average EEG signals using the 1-50 trials, 51-100 trials and 1-100 trials for normal and scrambled face stimuli.

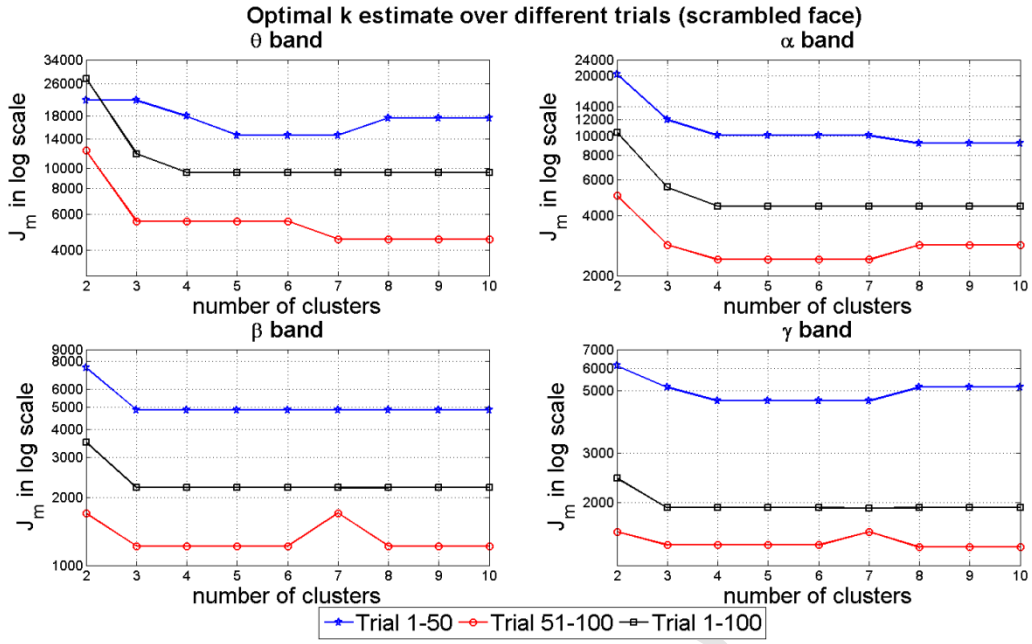

Figure 6: Cost functions for clustering in different EEG bands with increasing k during scrambled face perception.

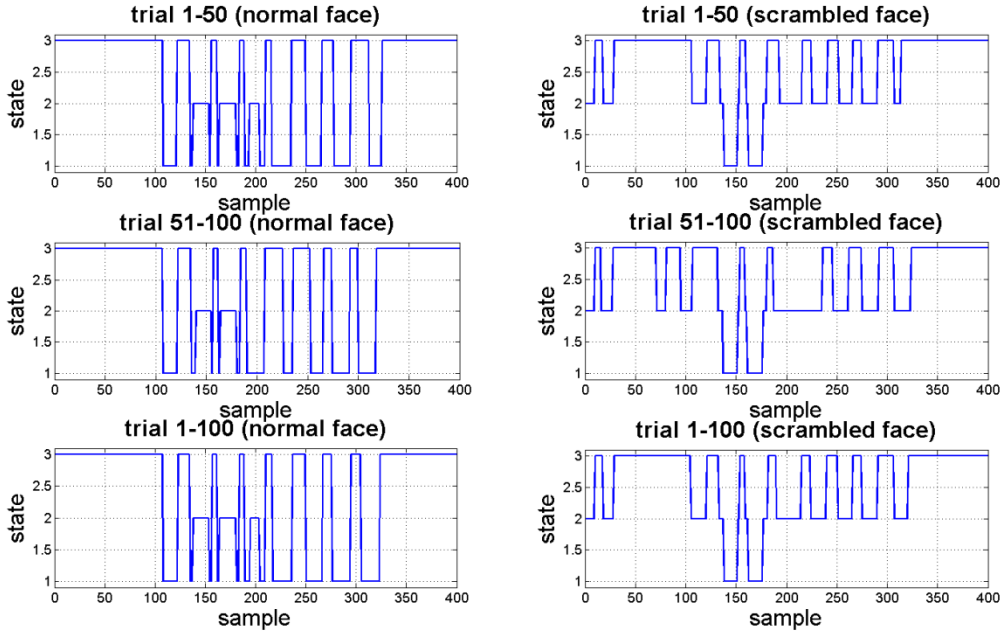

Figure 7: β band temporal evolution of synchrostates for different trials of EEG during normal and scrambled face perception.

Also it can be noted that the inter-synchrostate transition in Figure 7 occurs abruptly which is again similar to the transitional nature of the microstates [65]. Assuming that each task can be broken down into a sequence of subtasks, the time duration of each synchrostate in the time-course sequence may be indicative to the processing time required by the underlying brain circuitry for a subtask. In addition, the sequence and duration in which the synchrostates occur may reflect the sequence and time of information exchange that is characteristic to a particular task [66]. Therefore analysis of synchrostates could be an effective tool for quantitatively characterizing information processing ability of brain in different neurophysiological disorders where information integration and processing speed are the biggest issues, by comparing the sequence and duration of the synchrostates with those in a control population.

Table 2: Number of Occurrence (time instants) for Three States in β Band with Scrambled Face Stimulus

EEG segments	State 1	State 2	State 3
trial 1-50	29	123	248
trial 51-100	31	155	214
trial 1-100	29	137	234
Mean	29.67	138.33	232

3.4. Consistency of the synchrostates in different ensembles of EEG trials during normal and scrambled face perception

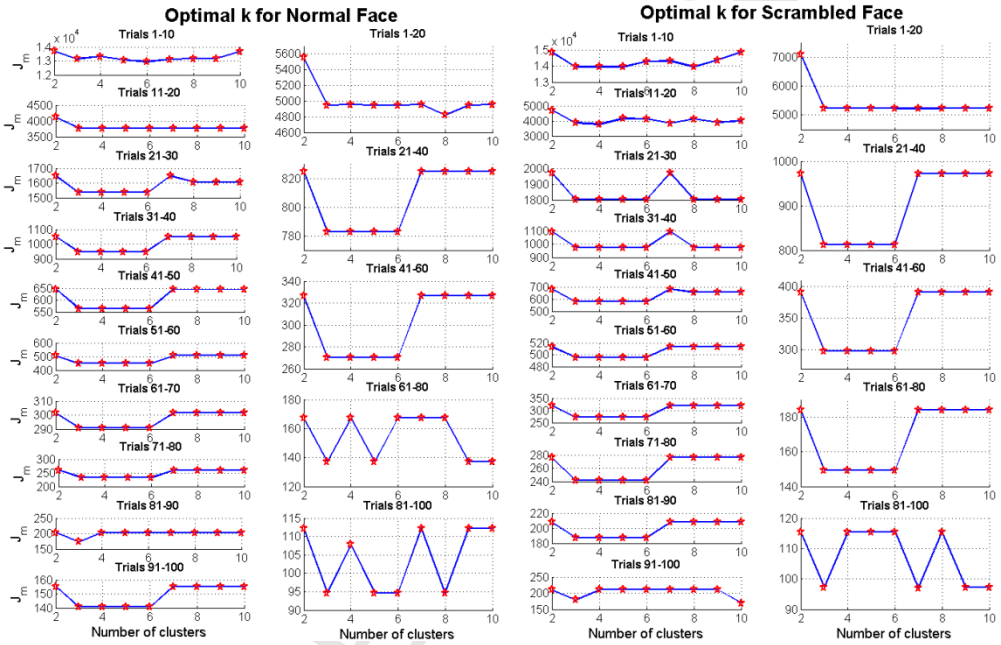

Figure 8: Determination of the optimum number of underlying synchrostates in the β band for different ensemble of EEGs during normal and scrambled face perception.

So far we reported the clustering results over large number of trials (50s and 100s). It may be argued that this may have possibly averaged out small inter-trial variability of the new physical phenomena i.e. the existence of synchrostates during normal and scrambled face perception. This is fundamental and worth looking at, in two different context of face perception task, to understand the basic physical nature of processing of these stimulus within the brain. We now verify that the number of unique patterns obtained in larger ensembles of EEG trials are consistent, in smaller groups as well. The clustering results that produce the optimal k estimates under normal and scrambled face stimuli have been reported here. The 100 trials of the 128 channel EEG are grouped into different ensembles as groups of 10s and 20s and then the clustering algorithm was run on each ensemble. Figure 8 shows that in each group of normal and scrambled face processing, we get three optimal synchrostates. These three unique states have been shown to be the same with larger ensembles as well (50s and all) as in Figure 1 and Figure 4. As discussed in Section 2.1, in different trials the characteristic knee can be found by the first significant fall in the cost function J_m. In some cases, there is an increase in the cost function indicating that the total sum of Euclidean

distances of all data points from the respective mean of clusters has increased due to splitting of large compact clusters into several smaller ones.

The fact of consistently obtaining three optimal states also confirms that the number of states obtained in the synchrostate analysis does not depend on how the data was divided in groups and on the choice of the number of trials used. Any stochastic process, such as EEGs are expected to have some inter-trial variability but the statistical measures, capturing the common underlying characteristics of different ensembles have been found to be the same. We have divided the 100 trials into larger subgroups (1 block of 100 and 2 blocks of 50) and smaller subgroups (5 blocks of 20 trials or 10 blocks of 10 trials) as well, to show that irrespective of the starting point, i.e. the number of trials the user selects at the beginning, a consistent number of synchrostates is still obtained.

3.5. Comparison of the connectivity analysis for normal and scrambled face

In order to gain a better insight into the implications of the synchrostates we construct complex networks corresponding to each of them. We have restricted our analysis in β band as it is more relevant to the information processing in the present case. The brain connectivity graphs and other relevant network measures, reported in this section are computed using the clustering results over all the ensembles (1-100 trials). While the EEG electrodes have been used as nodes, the synchronization indices Γ_{xy}, calculated using (6) are used as the edges connecting the $(x, y)^{th}$ nodes. The cross-electrode plots of Γ_{xy} are shown in Figure 9 where the close to unity value of Γ_{xy} (depicted as red color) indicates high degree of synchronization. This yields the basic connectivity matrix for the complex network analysis. From Figure 9 it is evident that there exist two distinct groups indicating good modularity in state 1 and state 2 – the smaller square box (electrodes 1-32) and the larger square box (33-128) – forming strongly connected groups amongst themselves with weak connections with the outside nodes.

In Figure 10 we translated the plots of Figure 9 into complex network structures. Owing to the property of Γ_{xy} the weight of the edges between the nodes not only describe the degree of synchronization amongst them (how well connected they are) but also the temporal stability of such synchronization. Figure 10 depicts the brain network structures for the normal face perception corresponding to each of the synchrostates 1, 2 and 3 respectively and also the same for the scrambled face scenario. All of the brain network plots have been made using the Gephi software [67]. For the ease of visualization only 7% amongst the highly connected edges are shown in Figure 10. The densely connected nodes are shown as the nodes with large diameters. As an example, the larger diameter of the node A6 in Figure 10 (state 1 of normal face) signifies higher connectivity than the relatively smaller diameter node A5. The connection strength to each node is based on the total connections to it before the 7% threshold was applied. Table 3 lists the results of our complex network analysis (without threshold) to obtain further insight into the functional organization of human brain at each of these states. The complex network measures in Table 3 have been computed using the brain connectivity toolbox [50] from the fully connected undirected graph.

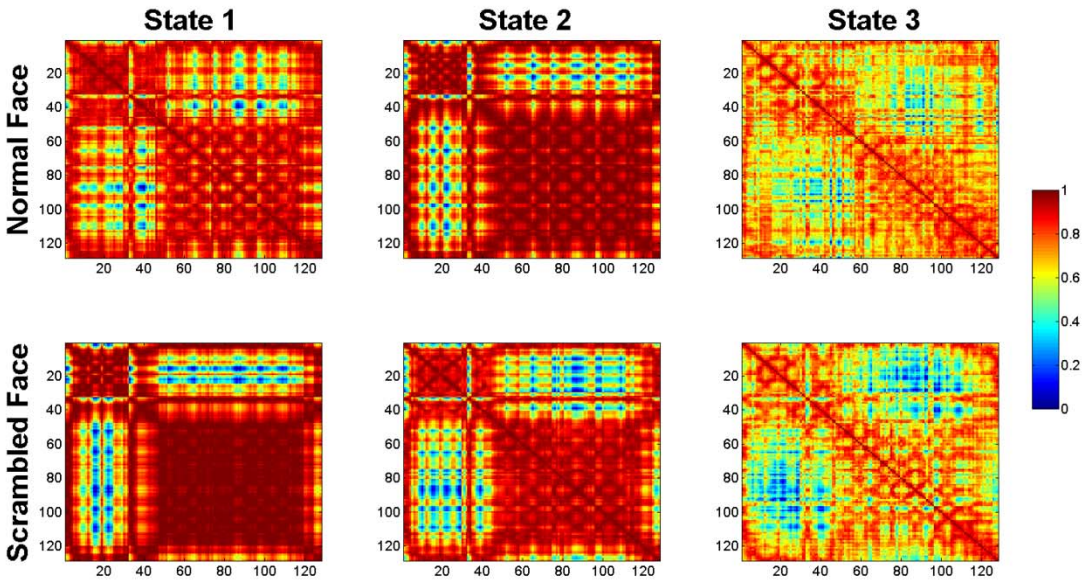

Figure 9: Synchronization index ($\Gamma_{x,y}$) or the connectivity weights between electrode pairs for different states with normal and scrambled face stimuli.

Table 3: Network measures for the brain connectivity corresponding to each synchrostate during normal and scrambled face perception (for trials 1-100)

Network measures	Normal face			Scrambled face		
	State1	State2	State3	State1	State2	State3
transitivity	0.9731	0.9015	0.9917	0.8325	0.9506	0.9906
modularity	0.0083	0.0339	0.0016	0.0649	0.0172	0.0022
characteristic path length	0.9579	0.8836	0.9761	0.6325	0.9362	0.9751
global efficiency	1.0367	1.1502	1.0165	1.9377	1.0631	1.0176
radius	0.9919	0.9119	0.9918	0.7136	0.9916	0.9918
diameter	0.9986	0.9988	0.998	0.9993	0.9981	0.9985

A discernible transition from one state to the other is clearly exhibited in these three state changes and is also reflected in the modularity and transitivity values. However, a close comparison of the modularity (or transitivity) values for each of the states in both the cases shows significant differences. The modularity value for normal face perception is the maximum for state 2 whereas for the scrambled face processing the maximum modularity is reflected in state 1. On the other hand the modularity values of state 3 for both of the cases are nearly same which is an order lower than the dominant modularity state in the two cases. One possible implication of this is that for normal and scrambled face processing, segregated specialized information processing within an area of highly-connected node assembly takes place in state 2 and state 1 respectively whereas in both of the cases, state 3 pertains to minimal specialized segregated processing. Visual observation of connectivity maps depicted in Figure 10 also confirms this observation where these highly connected nodal assemblies could be identified. As an example, a comparison of Figure 10 (a) and (b) clearly shows that

state 1 for scrambled face processing (Figure 10 (b)) shows denser connections between the nodes in the frontal and parietal regions compared to state 1 for normal face processing (Figure 10 (a)) and also exhibits less connectivity between this region and other regions of the brain. The effect is exactly opposite for state 2 (Figure 10(c) and (d)) where normal face processing shows denser connections than the scrambled one. The connectivity between different brain regions is less but more uniformly distributed for two cases of state 3 (Figure 10 (e) and (f)) than state 1 and state 2 confirming less value of modularity in Table 3.

From Table 3, observing the two major indices of information integration capability in a complex network – global efficiency and characteristic path length – once again a similar behavior has been found. Here, state 2 and state 1 possess larger global efficiency and smaller characteristic path length for the normal and scrambled face perceptions respectively, compared to those for the two cases of state 3 which indicate towards maximum information integration ability in these two states which affirms the study by Straaten and Stam [68]. It is also apparent from Table 3 that for state 2 of the normal face and state 1 of the scrambled face, the radius is the minimum. This implies that the graph is strongly connected and more information can flow very quickly from one region to the other due to lower radius and therefore resulting in more information integration ability in these states. The respective stability periods for each of these states may determine the time spent in global information exchange allowable by that state. During these periods the brain network is configured to share more information between distant nodes with ease. Combining these observations with the conclusions drawn from the values of modularity and transitivity, it is apparent that state 2 and state 1 represent dominant information processing states for normal and scrambled face processing respectively. These parameters can assess the efficiency or extent to which optimal partitioning occurs in the functional organization of brain [69][70].

However, although state 2 in normal face perception exhibits higher global efficiency and minimum characteristic path length, their values are still comparable with those in the other two states. Similar observation is true for the radius as well. This indicates that although state 2 is dominant for information integration, the other states also contribute to a comparable level for that process. However, modularity value of state 2 is significantly higher than that of the other states indicating the majority of segregated specialized processing taking place in this state. On the other hand, the above-mentioned parameter values for state 1 of scrambled face perception case are significantly different from those of the other two states indicating its dominance in both the processes of segregated information processing, (represented by high modularity) and information integration (small characteristic path length and high global efficiency). This supports the study by Stam [71] that modularity reflects segregation and characteristic path length indicates towards integration. Another interesting point to observe is that the information integration indices for the non-dominant states in the case of scrambled face processing show comparable values with even the dominant state (state 2) for normal face perception. This may mean that in general the information integration process required for scrambled face processing is more intense compared to that of the normal face processing. This is also evident from the significant difference of the network parameter values corresponding to state 1 of scrambled face processing among all 6 states (3 for normal face and 3 for scrambled face) in Table 3 *viz.* lowest transitivity, highest modularity, lowest characteristic path length, highest global efficiency and lowest radius. This argument also matches with our intuitive and practical understanding of the problem that a person will need greater attention or require more information integration to discern the scrambled face and therefore confirms the task-specific nature of information integration.

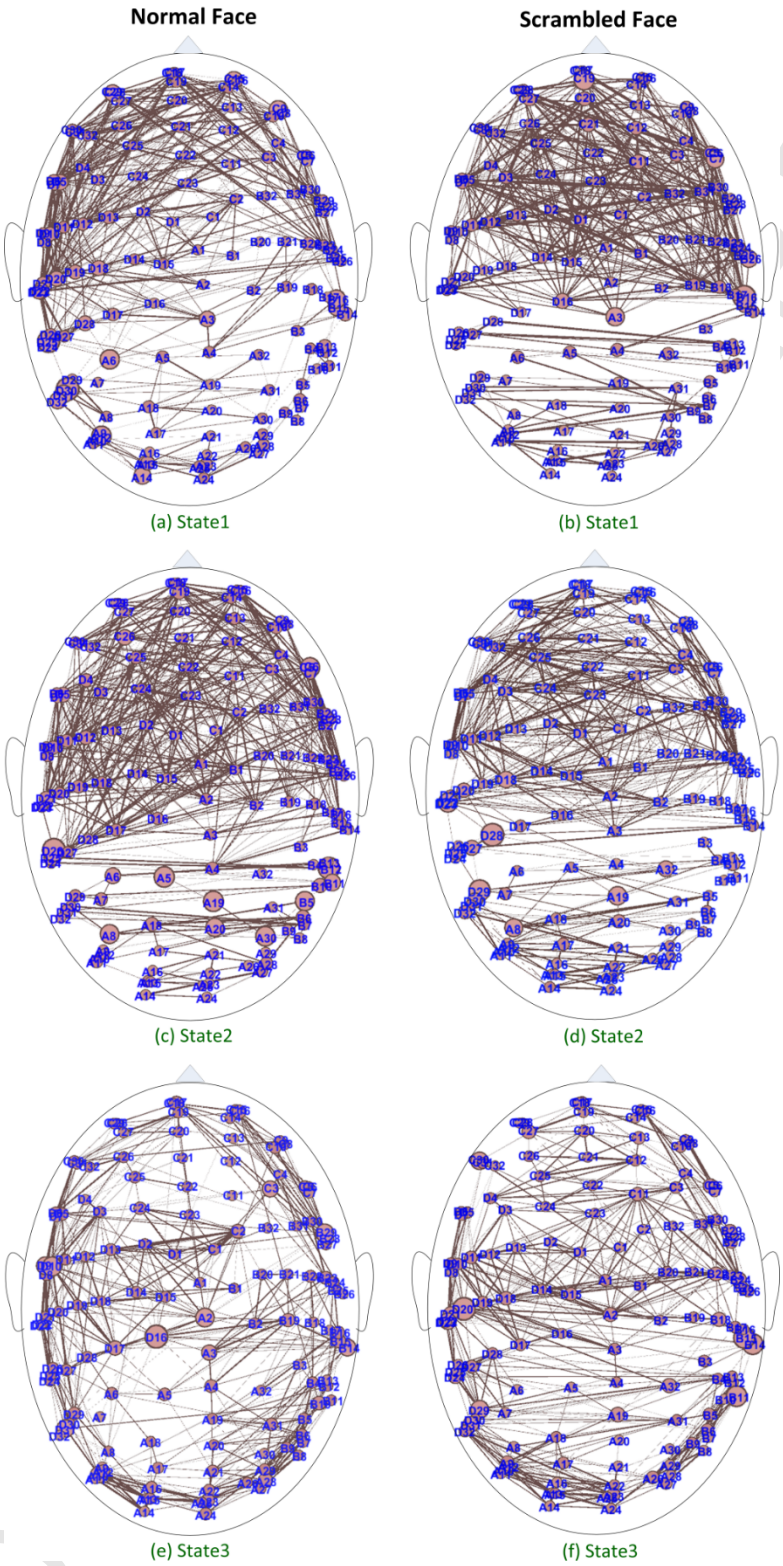

Figure 10: Single subject brain connectivity plots of three synchrostates for normal face and scrambled face stimuli in the β band.

The complete data processing workflow of extracting synchrostates from EEG and then measuring phase synchronization to generate brain connectivity plots to conduct graph-theoretic analysis is shown in Figure 11.

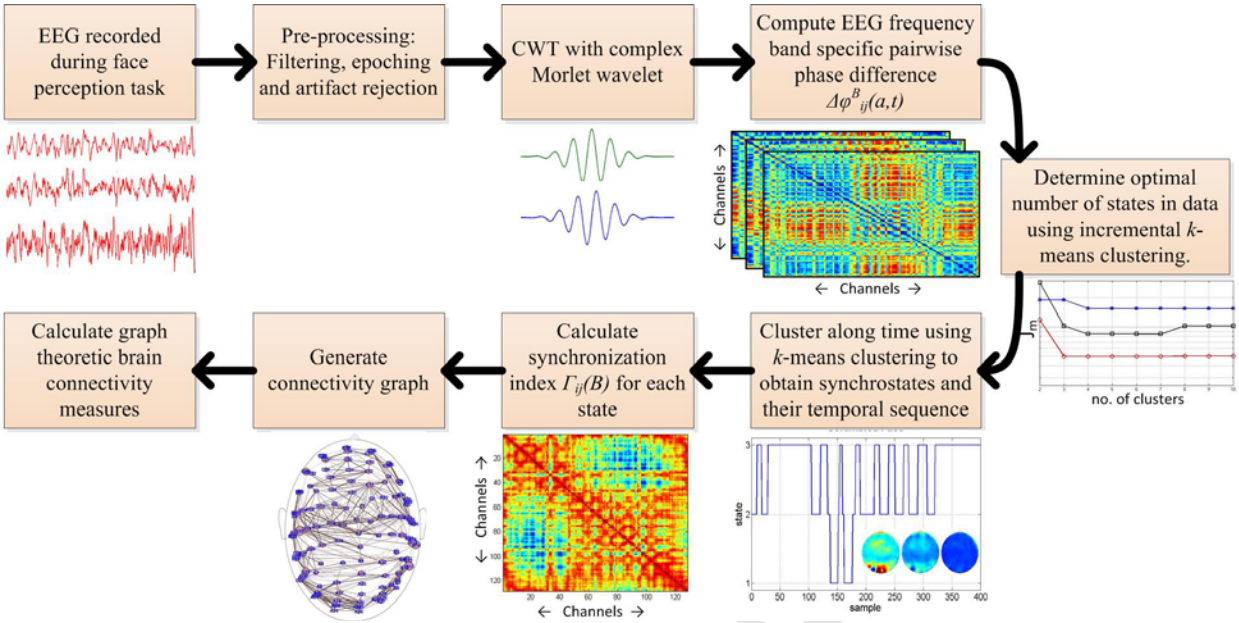

Figure 11: Flowchart of the data processing steps involved in the methodology for characterizing information processing in human brain through synchrostates.

3.6. Synchrostate and connectivity analysis of multiple subjects involving multiple trials during face perception

The results shown in the foregoing section are mainly based on a single subject multiple trail EEG. In order to explore whether the result holds true for a number of different subjects we apply the same procedure shown in Figure 11 on EEG recorded from 10 young adult subjects - 3 females and 7 males aged 26 to 31, when they were presented with three types of face perception stimuli i.e. famous face, scrambled face and unfamiliar face. An example of these stimuli is shown in the supplementary material. We used the data available in Henson *et al.* [37] where EEG was recorded simultaneously from 70 electrodes at 1.1 kHz, with the recording reference set at the nose electrode. The data was epoched from -200 ms to 600 ms to produce 100 trails for each subject and subsequently was pre-processed, filtered and artifact rejected, using the same algorithms and criteria used in the previous single subject study. The results presented in this section show the average synchrostate response of the 10 subjects which were obtained by taking the mean response of the 100 trials of each stimulus of each of the ten individuals.

Using the mean EEG of the 10 adults and following the steps to generate the optimal states using *k*-means clustering from the wavelet based time-frequency domain decomposition of the EEG signals, we obtained the results shown in Figure 12. For all the three stimuli (famous, scrambled and unfamiliar), the α, β and γ-band - all cluster at 5, 3 and 4 respectively, as the first significant 'knee' is observed at these values. In the θ band however, the famous face stimulus yields four optimal states where as the other two (scrambled and unfamiliar) stimuli have five optimal synchrostates. To corroborate our results from the single subject study reported in previous section, we now detail the results of the β-band synchrostate analysis for multiple subject group analysis.

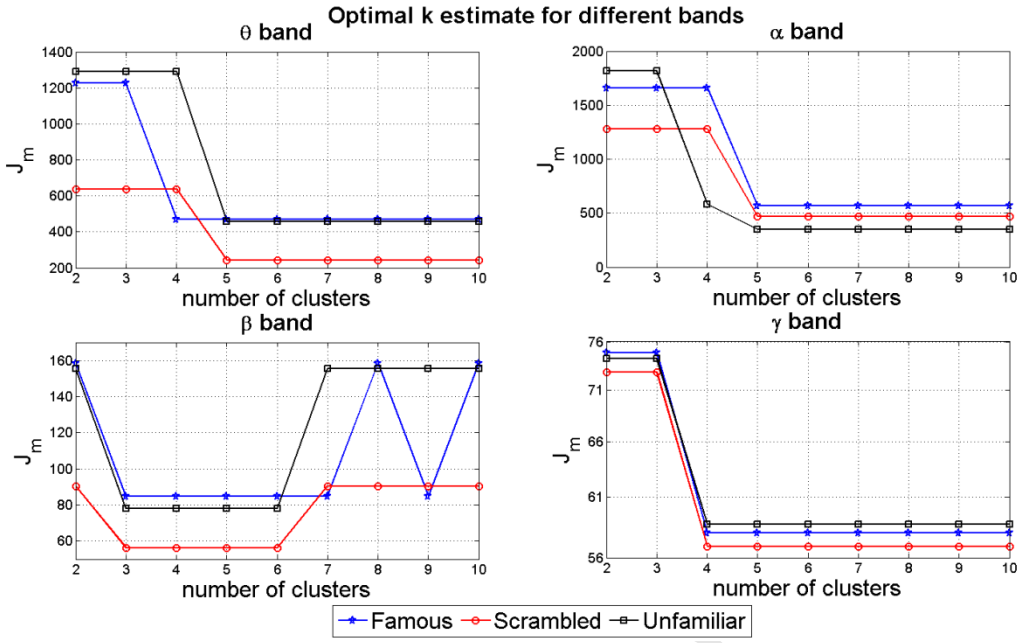

Figure 12: Determination of the optimum number of underlying clusters for different EEG bands during famous, scrambled and unfamiliar face perception for 10 subject group analysis.

Since this study is focused on the β band response, the head-plots for the synchrostates and their transitions for all the three stimuli (in this band) have been reported in Figure 13. As confirmed from Figure 12 the optimal number of synchrostates for all three stimuli is 3 in β band. The corresponding unique phase topographies or head-plots (Figure 13) show that for the general task of perceiving a face, be that famous or unfamiliar, the synchrostate topographies for both the famous face and the unfamiliar face are comparable. However, when perceiving the scrambled face, the state topography is different. The transition plots in Figure 14 show the 363 ms post stimulus response. The state labels between both experiments are arbitrarily labelled, so state 1 in experiment 1 (single subject analysis) is not analogous to state 1 in the second (group analysis). It is evident from Figure 14 that both famous and unfamiliar faces have similar transient synchrostate switching dynamics and response. However, similar to the conclusion from the face perception study, discussed earlier, it appears that for this pool of subjects as well, the state transitions are different for the general category of normal face (famous and unfamiliar faces) and scrambled face. These observations obtained from the results of 10 subjects, during a different experiment, affirm the phenomena of the existence of the synchrostates and the consistency in the results. The number of occurrence of each of the three states in the β band for all three stimuli has been reported in Table 4. Following on from the previous study, the synchronization index given in (6) is used to derive the connectivity diagram for the states which have been shown graphically in Figure 15 where only the strongest 7% amongst all the connections are shown. These results show that, without the loss of generality the same synchrostate analysis approach can be applied to an average subject group with multiple trials and also a single subject from EEG recorded over multiple trials.

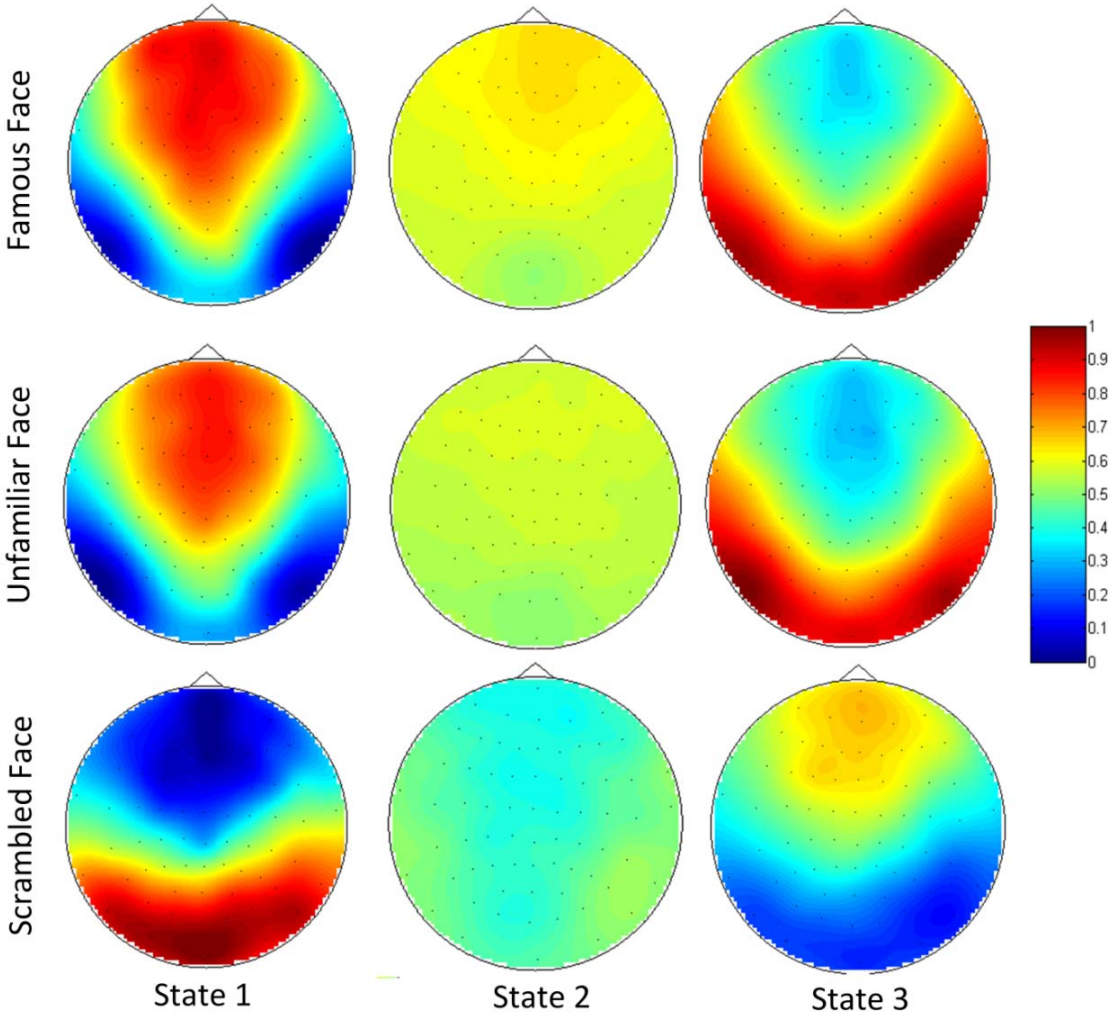

Figure 13: Multiple-subject average synchrostates during famous, unfamiliar and scrambled face perception in the β band.

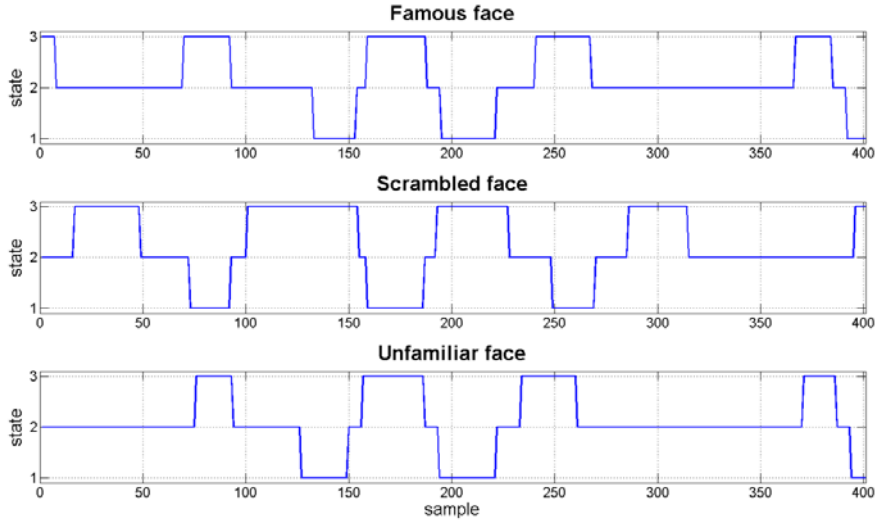

Figure 14: Multiple-subject averaged temporal evolution of β band synchrostates for three different face stimuli.

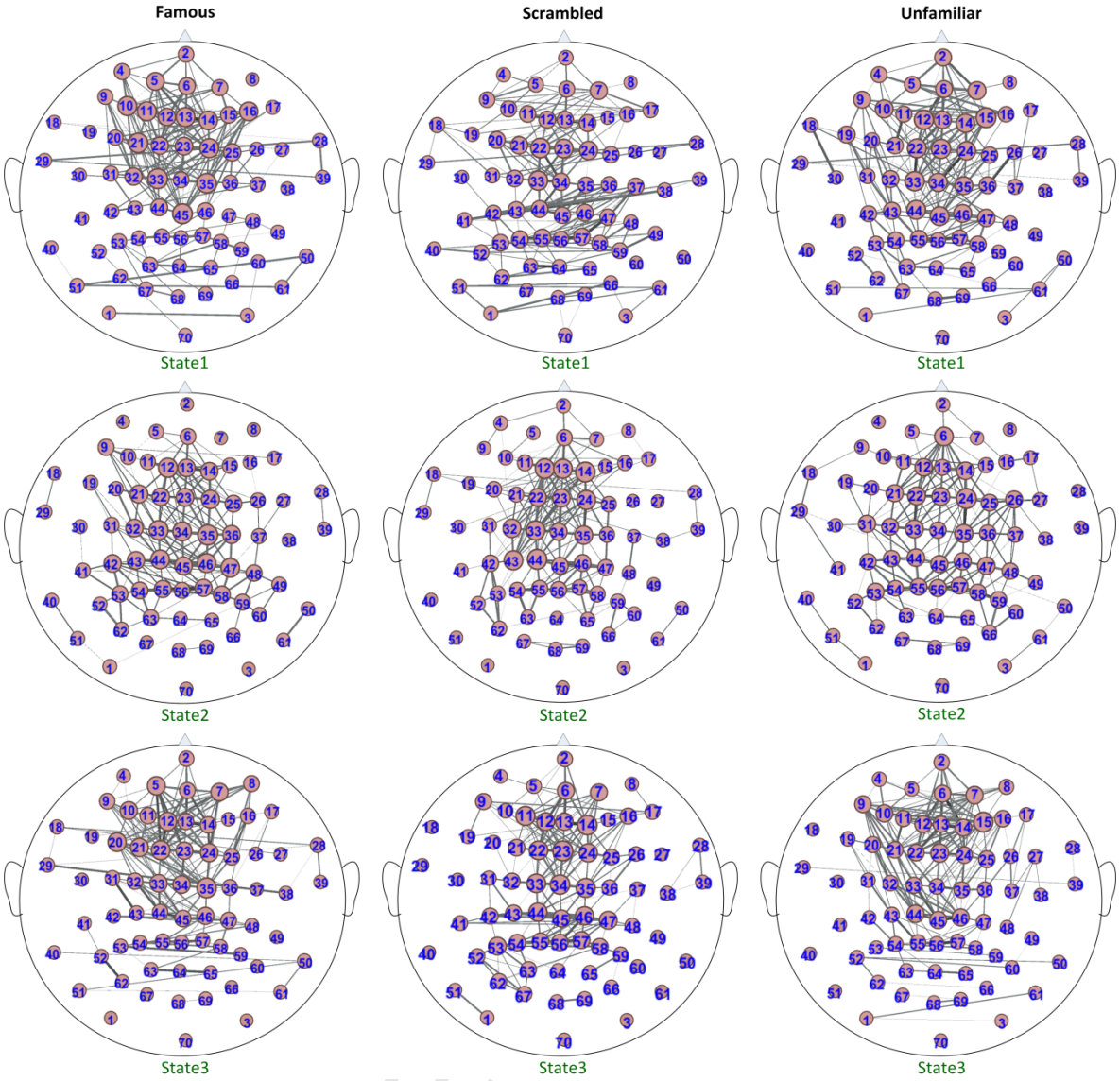

Figure 15: Brain connectivity plots of three synchrostates for famous face, scrambled face and unfamiliar face from multiple-subject averaged EEG in the β band.

Table 4: Number of occurrence of the three synchrostates in β band with three different face stimuli in the multiple-subject averaged EEG

Face stimuli	State 1	State 2	State 3
Famous	58	239	104
Scrambled	69	176	156
Unfamiliar	59	251	91

From our results, we conclude that there exist a small number of states which might have different topography in a face perception task. The results from the individual study show that the synchrostate properties are almost consistent across different trials from the same individual. The similarity between the group analysis and the individual analysis shows that the number of states is consistently three for both the cases, although the synchrostate topographies seems to be different due to difference in number of electrodes, electrode layout

as well as the sampling rate of EEG acquisition. Even for the group analysis, the synchrostate properties and transition plots amongst different individuals could be slightly different within one experimental paradigm and can be explored in future research.

4. Discussion

4.1. Synchrostate as a new EEG phase synchronization analysis and functional connectivity assessment tool

As shown from the foregoing discussion and data analysis, the existence of a small number of unique phase synchronized patterns or 'synchrostates' in multi-channel EEG system during visual stimuli is a new finding similar to the phenomenon observed in EEG potential which has been popular as 'microstates'. We have also shown that such synchrostates shows different transition characteristics depending on the nature of the stimuli and hence may characterize the brain dynamics in a task specific way. The formulation of the quasi-stable phase topographies is an intermediate step of the phase synchrony analysis and derivation of the final functional connectivity graphs [4]. The phase synchronized topographies (Figure 2, 5, 13) along with the temporal switching diagrams (Figure 7 and 14) forms the basis of the connection strengths in Figure 10 and 15, using the synchronization index. The translation of the synchrostates to produce brain connectivity and using connectivity or complex-network measures to characterize the stimulus are systematically presented in this paper. There have been recent studies on time-frequency analysis based dynamic functional connectivity modelling [72][73][74] which are based on spectral power analysis. The fundamental difference between the present study and [72][73][74] is that our study explores the evolution and organization of cognitive states or synchrostates that switch amongst themselves during the execution of the task. The states in the study in Lu *et al.* [72] are predefined states of a task (like a movement task) unlike ours where we use an unsupervised learning technique to find the synchrostates. Mehrkanoon *et al.* [74] mentions that the method they consider uses the information present in both the amplitude and phase fluctuations which in essence is different to what we aim to achieve through our study of finding EEG phase synchronization patterns using clustering.

Also, it is well known that the brain connectivity could have been derived in the source level. Although source level connectivity has more reliable physiological interpretations, reconstructing source activity from EEG is intrinsically an ill-posed problem and is known to have infinite solutions [75][76]. It suffers from the issue that using only EEG one cannot uniquely determine the spatial configuration of the underlying neural activity. Thus to resolve this issue with the inverse problem, one has to make a lot of assumptions about the problem to obtain an optimal and unique solution [77] and thus it only leads to approximate solutions [77]. Theoretically, only an infinite number of recording sites on the scalp would enable the determination of a unique location of the responsible sources inside [78]. The accuracy with which a source can be localized is affected by a number of factors like conductivity values and distribution, head-modelling, co-registration etc. [79][80]. Correct modelling of head tissue conductivities, as well as forward head model employed can be a source of error in such a problem [81]. Since the localized nodes within the brain are non-unique, connectivity analysis based on these nodes are still unreliable and based on some a priori assumptions that are made [80].

Also, due to many shortcomings of the short-time Fourier transform (STFT) compared to the CWT in proper representation of the time-frequency spectrum of a non-stationary signal like EEG, we restricted our study with CWT only, before the clustering were performed. It is well known that similar results could be obtained using STFT as well, just like using CWT, although there would be several heuristic factors like optimal choice of the

length of time window, choice of window function, degree of overlap etc. to consider. While performing CWT only the basis function needs to be chosen which slightly modifies the final result, whereas for STFT the choice of the aforementioned parameters (especially the length of the time window) completely changes the time-frequency representation of the non-stationary signal.

It is to be noted that our approach should not be confused with standard neuroimaging approaches which map the brain electrical potential (as a function of time) or the average spectral power over the scalp. The presented results indicate towards the existence of discrete phase synchronized 'states' that show stimulus-dependent time course of stability [66]. Therefore combining these two aspects we proposed a possible method of formulating connectivity from which a set of parameter could be extracted for quantifying cognitive functionality. In essence, we show that it would be possible to quantify the stochastic EEG response for such cognitive activities in terms of a few discrete states with switching amongst them. This reductionist approach of mapping stochastic time domain signals in terms of probabilistic switching between a small number of discrete states may have long term implication towards mathematical modeling and quantitative understanding of the human brain. The concept of reported semi-deterministic *synchrostates* in a stochastic multivariate time-series data (in multi-channel EEG) and translating these states to complex networks to characterize the stimulus would attract the attention of other sub-branches of statistical physics. The proposed methodology of finding EEG synchrostates and the associated connectivity may be utilized in various future applications especially in the domain of BCI [82] and diagnosis of neurodegenerative diseases [66], [83].

4.2. Investigating the effect of volume conduction on synchrostate analysis

The validity of phase synchrony, derived from EEG signals recorded over the scalp has been doubted in past literatures, as it is considered as the effect of spurious synchronization that occur due to volume conduction [84]. Studies which model the effect of distance between scalp electrodes suggest that the effects of volume conduction registered phase synchrony is significantly reduced at a distance of 4 cm [84][85]. Some papers state spurious coherence from volume conduction dropping to near zero when scalp electrodes were separated by 4 cm or more [86]. This can lead to difficulties in distinguishing between volume conduction and true synchrony in the short range (<4 cm) and limits the understanding of short range synchrony. Our results in the brain connectivity diagram (Figure 10 and Figure 15) show that most of the strong synchrony or connections are between distant electrodes which cannot be accounted for due to volume conduction. Only 9.4% (with a standard deviation of 2.1) of the synchronies reported here were between recording sites that are <4 cm apart. The rest of the connections (approximately 90.6%) and interactions are between electrodes with a distance > 4 cm. Such long range connections cannot be explained with volume conduction.

Electrical events inside of the human brain spread nearly instantaneously throughout any volume, like membranes, skin, tissues etc. Phase delays measured from spontaneous EEG can eliminate volume conduction since it is defined by zero phase difference everywhere in the volume [87]. Thus zero phase lag is characteristic of volume conduction and interactions reported from them are not reliable, whereas the network properties are measured through phase differences [87]. Volume conduction involves zero phase delays between any two points within the electrical field as collections of dipoles oscillate in time [88]. Zero phase delay is an important property of volume conduction based on which measures such as imaginary spectrum, bi-coherence, phase reset and coherence of long phase delays are considered critical in measuring brain connectivity, independent of volume conduction

[11][89][90]. According to the assumptions in pioneering paper regarding identifying true brain interaction by Nolte *et al.* [11], phase shifts (phase differences) cannot be explained by volume conduction. In our paper from the very beginning we use the same premise and only cluster similar phase difference matrices. Therefore it can be concluded that the synchrostates cannot be explained by volume conduction. The synchrony observed in our study does not report zero phase lag synchronization. Also, as per the study of Stam *et al.* [91], the existence of a consistent non-zero phase lag cannot be explained by volume conduction. The non-zero value of pair-wise phase differences along time in our study, suggests that the synchronies are not artifactual hence is a reflection of brain interactions and is not a result of volume conduction.

Another property of synchrostates that cannot be explained by volume conduction is the desynchronization and resynchronization [92] of different electrode signals over time i.e. the transition between the states in ms order. If the synchrony captured was in fact the effect of volume conduction it does not account for the change in the synchronization pattern in both strength and between relative electrodes over time (in ms) during state changes. Synchrony resulting from volume conduction would result in constant synchronization configuration prevailing over the scalp throughout the recording time for all the synchrostates. Even the signals from a single intermittent source will simultaneously affect all the electrode recordings. Thus time delays between electrodes cannot be accounted for by a single intermittent source [93][94]. If the single source activity was conducted through a distributed lead field its intermittent activation patterns would also be volume conducted to several of scalp electrodes. Such a scenario would entail there would be no change in the effective phase difference between two electrode signals during these intermittently active sources [92]. Stam *et al.* [91], states that the asymmetric distribution of instantaneous phase differences between two signals cannot be explained by volume conduction from a single source. The time varying desynchronizing and resynchronizing nature of the synchrostates is due to the asymmetric nature of the reported phase differences which causes $\Delta\varphi_{xy}(a,t)$ to be sometimes positive or negative and larger or smaller indicating towards a phase lag and a phase lead and hence changes the synchronization pattern between electrodes as a result. The phase difference between a pair of electrodes abruptly change and then can reconfigure into new topographies which confirms that the synchrostates are not affected by volume conduction. The asymmetry in the distribution of synchrony and connections in Figure 10 and Figure 15 also affirms this conclusion.

If volume conduction creates high synchrony between two electrodes, then the high synchrony should also be observed between all the neighbouring electrodes [16] throughout the synchrostate analysis (high synchrony among neighbouring electrodes throughout time), however this is not the case as can be seen from the connectivity maps in the Figure 10 and Figure 15. The patterns of synchrony are non-homogenous and change with time and for every synchrostate. The synchrony between neighbouring electrodes change and in some cases become insignificant resulting in different connection strengths. We conclude that these observations are convincing evidence that significant long-range synchronies are established during this cognitive task as these synchronies cannot be explained by volume conduction; it seems more likely that they represent an association of the functional integration mechanism during visual perception tasks. For more details on the effect of volume conduction, please refer to the supplementary material.

Research has established and stressed on the idea that the phenomenon of phase synchrony over the scalp extends to dynamic brain mapping [92]. Information processing between neural assemblies with similar dynamical functional state is facilitated by synchronized oscillatory activity of the neural groups. Deeper understanding of this

integration process between such groups during cognitive tasks can be useful in describing brain organization [95].

5. Conclusion

In our exploration, existence of consistent synchrostates in the β-band over 100 trials of EEG signals under a normal and scrambled face perception scenario have been reported. This result has led to the observation of unique phase synchronized patterns or states, in a single subject and also a group of 10 adults. The temporal evolution of these states are also unique and depends on the type of stimuli. From our study, the fact of consistently obtaining synchrostates in β band is in conformation with the contemporary literatures that reports a direct relationship of this band with visual perception tasks. The unique and repetitive time-course of inter-synchrostate switching reflects the temporal dynamics of the underlying interactions amongst the brain region and therefore may be considered as the characteristic feature for a specific task. Our exploration on the single adult, shows that although two different tasks (here normal and scrambled face perception) may belong to the same category (visual processing in general), depending on the nature of stimulus, the inter-synchrostate switching dynamics is markedly different between them. Complex network analysis for the temporal stability and the nature of the synchrostates has been found to be effective in objectively measuring the characteristic interactions in terms of specialized segmented processing and information integration.

Therefore comparison of the resulting metrics along with the inter-synchrostate switching time-course between a normal and a neurologically impaired subject in a task-specific manner is expected to reveal the information processing impairments in the latter, leading to a methodology for person-specific characterization of neurological anomalies, given the EEG data. However, it is to be noted that in this work, we have carried out exploration for face-perception task only. Therefore whether the observed nature of synchrostate behavior is consistent for other tasks, both in typical and neurologically impaired subject, needs further exploration.

References

[1] J. Fell and N. Axmacher, “The role of phase synchronization in memory processes,” *Nature Reviews Neuroscience*, vol. 12, no. 2. pp. 105–118, 2011.

[2] B. Horwitz, “The elusive concept of brain connectivity,” *NeuroImage*, vol. 19, no. 2. pp. 466–470, 2003.

[3] O. Sporns, *Networks of the Brain*. MIT press, 2011.

[4] W. Jamal, S. Das, I.-A. Oprescu, K. Maharatna, F. Apicella, and F. Sicca, “ Classification of autism spectrum disorder using supervised learning of brain connectivity measures extracted from synchrostates.,” *Journal of Neural Engineering*, vol. 11, no. 4. p. 046019, 2014.

[5] R. Q. Quiroga, A. Kraskov, T. Kreuz, and P. Grassberger, “Performance of different synchronization measures in real data: a case study on electroencephalographic signals,” *Physical Review E*, vol. 65, no. 4. p. 041903, 2002.

[6] A. K. Engel, P. Fries, and W. Singer, “Dynamic predictions: oscillations and synchrony in top-down processing,” *Nature Reviews Neuroscience*, vol. 2, no. 10. pp. 704–716,

2001.

[7] C. M. Gray, P. K□nig, A. K. Engel, and W. Singer, "Oscillatory responses in cat visual cortex exhibit inter-columnar synchronization which reflects global stimulus properties," *Nature*, vol. 338, no. 6213. pp. 334–337, 1989.

[8] P. Fries, J. H. Reynolds, A. E. Rorie, and R. Desimone, "Modulation of oscillatory neuronal synchronization by selective visual attention," *Science*, vol. 291, no. 5508. pp. 1560–1563, 2001.

[9] L. Leocani, C. Toro, P. Manganotti, P. Zhuang, and M. Hallett, "Event-related coherence and event-related desynchronization/synchronization in the 10 Hz and 20 Hz EEG during self-paced movements," *Electroencephalography and Clinical Neurophysiology/Evoked Potentials Section*, vol. 104, no. 3. pp. 199–206, 1997.

[10] S. Weiss and P. Rappelsberger, "Long-range EEG synchronization during word encoding correlates with successful memory performance," *Cognitive Brain Research*, vol. 9, no. 3. pp. 299–312, 2000.

[11] G. Nolte, O. Bai, L. Wheaton, Z. Mari, S. Vorbach, and M. Hallett, "Identifying true brain interaction from EEG data using the imaginary part of coherency," *Clinical Neurophysiology*, vol. 115, no. 10. pp. 2292–2307, 2004.

[12] F. Varela, J.-P. Lachaux, E. Rodriguez, and J. Martinerie, "The brainweb: phase synchronization and large-scale integration," *Nature Reviews Neuroscience*, vol. 2, no. 4. pp. 229–239, 2001.

[13] F. Mormann, K. Lehnertz, P. David, and C. E Elger, "Mean phase coherence as a measure for phase synchronization and its application to the EEG of epilepsy patients," *Physica D: Nonlinear Phenomena*, vol. 144, no. 3. pp. 358–369, 2000.

[14] A. Hillebrand, G. R. Barnes, J. L. Bosboom, H. W. Berendse, and C. J. Stam, "Frequency-dependent functional connectivity within resting-state networks: an atlas-based MEG beamformer solution," *NeuroImage*, vol. 59, no. 4. pp. 3909–3921, 2012.

[15] L. Astolfi and F. Babiloni, *Estimation of cortical connectivity in humans*. Morgan and Claypool, 2008.

[16] J.-P. Lachaux, E. Rodriguez, J. Martinerie, F. J. Varela, and others, "Measuring phase synchrony in brain signals," *Human Brain Mapping*, vol. 8, no. 4. pp. 194–208, 1999.

[17] M. G. Rosenblum, A. S. Pikovsky, and J. Kurths, "Phase synchronization of chaotic oscillators," *Physical Review Letters*, vol. 76, no. 11. p. 1804, 1996.

[18] K.-H. Lee, L. M. Williams, M. Breakspear, and E. Gordon, "Synchronous gamma activity: a review and contribution to an integrative neuroscience model of schizophrenia," *Brain Research Reviews*, vol. 41, no. 1. pp. 57–78, 2003.

[19] K. Lehnertz et al., "Seizure prediction by nonlinear EEG analysis," *Engineering in Medicine and Biology Magazine, IEEE*, vol. 22, no. 1. pp. 57–63, 2003.

[20] S. K. Esser, S. L. Hill, and G. Tononi, "Sleep homeostasis and cortical synchronization: I. Modeling the effects of synaptic strength on sleep slow waves," *Sleep*, vol. 30, no. 12. p. 1617, 2007.

[21] K. Maharajh, P. Teale, D. C. Rojas, and M. L. Reite, "Fluctuation of gamma-band phase synchronization within the auditory cortex in schizophrenia," *Clinical Neurophysiology*, vol. 121, no. 4. pp. 542–548, 2010.

[22] S. Phillips and Y. Takeda, "Frontal-parietal synchrony in elderly EEG for visual search," *International Journal of Psychophysiology*, vol. 75, no. 1. pp. 39–43, 2010.

[23] M. Le Van Quyen et al., "Comparison of Hilbert transform and wavelet methods for the analysis of neuronal synchrony," *Journal of Neuroscience Methods*, vol. 111, no. 2. pp. 83–98, 2001.

[24] A. Y. Mutlu, E. Bernat, and S. Aviyente, "A Signal-Processing-Based Approach to Time-Varying Graph Analysis for Dynamic Brain Network Identification," *Computational and Mathematical Methods in Medicine*, vol. 2012. 2012.

[25] F. D. V. Fallani et al., "Persistent patterns of interconnection in time-varying cortical networks estimated from high-resolution EEG recordings in humans during a simple motor act," *Journal of Physics A: Mathematical and Theoretical*, vol. 41, no. 22. p. 224014, 2008.

[26] "Multimodal face-evoked dataset." [Online]. Available: http://www.fil.ion.ucl.ac.uk/spm/data/mmfaces/.

[27] Y. Sugita, "Innate face processing," *Current Opinion in Neurobiology*, vol. 19, no. 1. pp. 39–44, 2009.

[28] R. Adolphs, "Recognizing emotion from facial expressions: Psychological and neurological mechanisms," *Behavioral and Cognitive Neuroscience reviews*, vol. 1, no. 1. pp. 21–62, 2002.

[29] T. Kaufmann, S. Schulz, C. Grünzinger, and A. Kübler, "Flashing characters with famous faces improves ERP-based brain-computer interface performance," *Journal of Neural Engineering*, vol. 8, no. 5. p. 056016, 2011.

[30] Y. Zhang, Q. Zhao, J. Jin, X. Wang, and A. Cichocki, "A novel BCI based on ERP components sensitive to configural processing of human faces," *Journal of Neural Engineering*, vol. 9, no. 2. p. 026018, 2012.

[31] D. Lehmann, H. Ozaki, and I. Pal, "EEG alpha map series: brain micro-states by space-oriented adaptive segmentation," *Electroencephalography and Clinical Neurophysiology*, vol. 67, no. 3. pp. 271–288, 1987.

[32] F. Boiten, J. Sergeant, and R. Geuze, "Event-related desynchronization: the effects of energetic and computational demands," *Electroencephalography and Clinical Neurophysiology*, vol. 82, no. 4. pp. 302–309, 1992.

[33] B. Güntekin and E. Basar, "Emotional face expressions are differentiated with brain oscillations," *International Journal of Psychophysiology*, vol. 64, no. 1. pp. 91–100, 2007.

[34] E. Bacsar, C. Schmiedt-Fehr, A. Öniz, and C. Bacsar-Erouglu, "Brain oscillations evoked by the face of a loved person," *Brain Research*, vol. 1214. pp. 105–115, 2008.

[35] A. Wróbel, "Beta activity: a carrier for visual attention," *Acta Neurobiologiae Experimentalis*, vol. 60, no. 2. pp. 247–260, 2000.

[36] J. Gross et al., "Modulation of long-range neural synchrony reflects temporal limitations of visual attention in humans," *Proceedings of the National Academy of Sciences of the United States of America*, vol. 101, no. 35. pp. 13050–13055, 2004.

[37] R. N. Henson, D. G. Wakeman, V. Litvak, and K. J. Friston, "A parametric empirical Bayesian framework for the EEG/MEG inverse problem: generative models for multi-subject and multi-modal integration," *Frontiers in Human Neuroscience*, vol. 5. 2011.

[38] W. Jamal et al., "Using brain connectivity measure of EEG synchrostates for discriminating typical and Autism Spectrum Disorder," in *Neural Engineering (NER), 2013 6th International IEEE/EMBS Conference on*, 2013, pp. 1402–1405.

[39] T. Peng, A. B. Rowley, P. N. Ainslie, M. J. Poulin, and S. J. Payne, "Wavelet phase synchronization analysis of cerebral blood flow autoregulation," *Biomedical Engineering, IEEE Transactions on*, vol. 57, no. 4. pp. 960–968, 2010.

[40] S. Theodoridis, A. Pikrakis, K. Koutroumbas, and D. Cavouras, *Introduction to Pattern Recognition: A Matlab Approach: A Matlab Approach*. Academic Press, 2010.

[41] S. Theodoridis and K. Koutroumbas, *Pattern Recognition*. Academic Press, 2009.

[42] K. Mardia and P. Jupp, "Directional statistics. 2000."

[43] E. Bullmore and O. Sporns, "Complex brain networks: graph theoretical analysis of structural and functional systems," *Nature Reviews Neuroscience*, vol. 10, no. 3. pp. 186–198, 2009.

[44] F. De Vico Fallani et al., "Brain network analysis from high-resolution EEG recordings by the application of theoretical graph indexes," *Neural Systems and Rehabilitation Engineering, IEEE Transactions on*, vol. 16, no. 5. pp. 442–452, 2008.

[45] L. Astolfi et al., "Neural basis for brain responses to TV commercials: a high-resolution EEG study," *Neural Systems and Rehabilitation Engineering, IEEE Transactions on*, vol. 16, no. 6. pp. 522–531, 2008.

[46] C. Cao and S. Slobounov, "Alteration of cortical functional connectivity as a result of traumatic brain injury revealed by graph theory, ICA, and sLORETA analyses of EEG signals," *Neural Systems and Rehabilitation Engineering, IEEE Transactions on*, vol. 18, no. 1. pp. 11–19, 2010.

[47] Y. He, Z. Chen, and A. Evans, "Structural insights into aberrant topological patterns of large-scale cortical networks in Alzheimer's disease," *The Journal of neuroscience*, vol. 28, no. 18. Soc Neuroscience, pp. 4756–4766, 2008.

[48] D. S. Bassett, E. Bullmore, B. A. Verchinski, V. S. Mattay, D. R. Weinberger, and A. Meyer-Lindenberg, "Hierarchical organization of human cortical networks in health and schizophrenia," *The Journal of Neuroscience*, vol. 28, no. 37. Soc Neuroscience, pp. 9239–9248, 2008.

[49] G. Tononi, O. Sporns, and G. M. Edelman, "A measure for brain complexity: relating functional segregation and integration in the nervous system," *Proceedings of the National Academy of Sciences*, vol. 91, no. 11. National Acad Sciences, pp. 5033–5037, 1994.

[50] M. Rubinov and O. Sporns, "Complex network measures of brain connectivity: uses and interpretations," *NeuroImage*, vol. 52, no. 3. pp. 1059–1069, 2010.

[51] S. H. Strogatz, "Exploring complex networks," *Nature*, vol. 410, no. 6825. pp. 268–276, 2001.

[52] O. Sporns, "Network attributes for segregation and integration in the human brain," *Current opinion in neurobiology*, vol. 23, no. 2. Elsevier, pp. 162–171, 2013.

[53] D. J. Watts and S. H. Strogatz, "Collective dynamics of 'small-world'networks," *Nature*, vol. 393, no. 6684. pp. 440–442, 1998.

[54] G. Tononi, G. M. Edelman, and O. Sporns, "Complexity and coherency: integrating information in the brain," *Trends in cognitive sciences*, vol. 2, no. 12. Elsevier, pp. 474–484, 1998.

[55] F. De Vico Fallani et al., "Community structure in large-scale cortical networks during motor acts," *Chaos, Solitons & Fractals*, vol. 45, no. 5. pp. 603–610, 2012.

[56] M. P. Van Den Heuvel and H. E. H. Pol, "Exploring the brain network: a review on resting-state fMRI functional connectivity," *European Neuropsychopharmacology*, vol. 20, no. 8. Elsevier, pp. 519–534, 2010.

[57] F. Musso, J. Brinkmeyer, A. Mobascher, T. Warbrick, and G. Winterer, "Spontaneous brain activity and EEG microstates. A novel EEG/fMRI analysis approach to explore resting-state networks," *NeuroImage*, vol. 52, no. 4. pp. 1149–1161, 2010.

[58] M. D. Fox, A. Z. Snyder, J. L. Vincent, and M. E. Raichle, "Intrinsic fluctuations within cortical systems account for intertrial variability in human behavior," *Neuron*, vol. 56, no. 1. Elsevier, pp. 171–184, 2007.

[59] A. Arieli, A. Sterkin, A. Grinvald, and A. Aertsen, "Dynamics of ongoing activity: explanation of the large variability in evoked cortical responses," *Science*, vol. 273, no. 5283. American Association for the Advancement of Science, pp. 1868–1871, 1996.

[60] D. J. McFarland, A. T. Lefkowicz, and J. R. Wolpaw, "Design and operation of an EEG-based brain-computer interface with digital signal processing technology," *Behavior Research Methods, Instruments & Computers*, vol. 29, no. 3. pp. 337–345, 1997.

[61] M. Fatourechi, A. Bashashati, R. K. Ward, and G. E. Birch, "EMG and EOG artifacts in brain computer interface systems: A survey," *Clinical Neurophysiology*, vol. 118, no. 3. pp. 480–494, 2007.

[62] P. Anderer et al., "Artifact processing in computerized analysis of sleep EEG-a review," *Neuropsychobiology*, vol. 40, no. 3. pp. 150–157, 1999.

[63] D. J. McFarland, L. M. McCane, S. V. David, and J. R. Wolpaw, "Spatial filter selection for EEG-based communication," *Electroencephalography and Clinical Neurophysiology*, vol. 103, no. 3. pp. 386–394, 1997.

[64] S. Yuval-Greenberg and L. Y. Deouell, "The broadband-transient induced gamma-band response in scalp EEG reflects the execution of saccades," *Brain Topography*, vol. 22, no. 1. pp. 3–6, 2009.

[65] M. Gärtner, V. Brodbeck, H. Laufs, and G. Schneider, "A stochastic model for EEG microstate sequence analysis," *NeuroImage*, vol. 104. pp. 199–208, 2015.

[66] W. Jamal, S. Das, I.-A. Oprescu, and K. Maharatna, "Prediction of Synchrostate Transitions in EEG Signals Using Markov Chain Models," *Signal Processing Letters, IEEE*, vol. 22, no. 2. pp. 149–152, 2015.

[67] M. Bastian, S. Heymann, and M. Jacomy, "Gephi: an open source software for exploring and manipulating networks.," in *ICWSM*, 2009, pp. 361–362.

[68] E. C. van Straaten and C. J. Stam, "Structure out of chaos: Functional brain network analysis with EEG, MEG, and functional MRI," *European Neuropsychopharmacology*, vol. 23, no. 1. pp. 7–18, 2013.

[69] O. Sporns, "From simple graphs to the connectome: networks in neuroimaging," *NeuroImage*, vol. 62, no. 2. pp. 881–886, 2012.

[70] M. Rubinov and O. Sporns, "Weight-conserving characterization of complex functional brain networks," *NeuroImage*, vol. 56, no. 4. pp. 2068–2079, 2011.

[71] C. Stam, "Characterization of anatomical and functional connectivity in the brain: a complex networks perspective," *International Journal of Psychophysiology*, vol. 77, no. 3. pp. 186–194, 2010.

[72] C.-F. Lu et al., "Reorganization of functional connectivity during the motor task using EEG time-frequency cross mutual information analysis," *Clinical Neurophysiology*, vol.

122, no. 8. pp. 1569–1579, 2011.

[73] C. Chang, Z. Liu, M. C. Chen, X. Liu, and J. H. Duyn, "EEG correlates of time-varying BOLD functional connectivity," *NeuroImage*, vol. 72. pp. 227–236, 2013.

[74] S. Mehrkanoon, M. Breakspear, and T. W. Boonstra, "Low-Dimensional Dynamics of Resting-State Cortical Activity," *Brain Topography*. pp. 1–15, 2013.

[75] S. Sanei and J. A. Chambers, *EEG signal processing*. John Wiley & Sons, 2008.

[76] R. D. Pascual-Marqui, "Review of methods for solving the EEG inverse problem," *International Journal of Bioelectromagnetism*, vol. 1, no. 1. pp. 75–86, 1999.

[77] C. Phillips, J. Mattout, M. D. Rugg, P. Maquet, and K. J. Friston, "An empirical Bayesian solution to the source reconstruction problem in EEG," *NeuroImage*, vol. 24, no. 4. pp. 997–1011, 2005.

[78] Z. J. Koles, "Trends in EEG source localization," *Electroencephalography and Clinical Neurophysiology*, vol. 106, no. 2. pp. 127–137, 1998.

[79] K. Whittingstall, G. Stroink, L. Gates, J. Connolly, and A. Finley, "Effects of dipole position, orientation and noise on the accuracy of EEG source localization," *Biomedical Engineering Online*, vol. 2, no. 1. p. 14, 2003.

[80] R. Grech et al., "Review on solving the inverse problem in EEG source analysis," *Journal of Neuroengineering and Rehabilitation*, vol. 5, no. 1. p. 25, 2008.

[81] Z. A. Acar and S. Makeig, "Effects of forward model errors on EEG source localization," *Brain Topography*, vol. 26, no. 3. pp. 378–396, 2013.

[82] J. Jin, B. Z. Allison, Y. Zhang, X. Wang, and A. Cichocki, "An ERP-based BCI using an oddball paradigm with different faces and reduced errors in critical functions," *International Journal of Neural Systems*, vol. 24, no. 08. 2014.

[83] T. Kaufmann, S. M. Schulz, A. K□blitz, G. Renner, C. Wessig, and A. Kübler, "Face stimuli effectively prevent brain-computer interface inefficiency in patients with neurodegenerative disease," *Clinical Neurophysiology*, vol. 124, no. 5. pp. 893–900, 2013.

[84] P. L. Nunez et al., "EEG coherency: I: statistics, reference electrode, volume conduction, Laplacians, cortical imaging, and interpretation at multiple scales," *Electroencephalography and Clinical Neurophysiology*, vol. 103, no. 5. pp. 499–515, 1997.

[85] P. L. Nunez et al., "EEG coherency II: experimental comparisons of multiple measures," *Clinical Neurophysiology*, vol. 110, no. 3. pp. 469–486, 1999.

[86] S. M. Doesburg, A. B. Roggeveen, K. Kitajo, and L. M. Ward, "Large-scale gamma-band phase synchronization and selective attention," *Cerebral Cortex*, vol. 18, no. 2. pp.

386–396, 2008.

[87] R. W. Thatcher, D. M. North, and C. J. Biver, "Development of cortical connections as measured by EEG coherence and phase delays," *Human Brain Mapping*, vol. 29, no. 12. pp. 1400–1415, 2008.

[88] P. Nunez and R. Srinivasan, "Electrical fields of the brain," *New York: Oxford*. 1981.

[89] R. D. Pascual-Marqui, "Coherence and phase synchronization: generalization to pairs of multivariate time series, and removal of zero-lag contributions," *arXiv preprint arXiv:0706.1776*. 2007.

[90] L. R. Peraza, A. U. Asghar, G. Green, and D. M. Halliday, "Volume conduction effects in brain network inference from electroencephalographic recordings using phase lag index," *Journal of Neuroscience Methods*, vol. 207, no. 2. pp. 189–199, 2012.

[91] C. J. Stam, G. Nolte, and A. Daffertshofer, "Phase lag index: assessment of functional connectivity from multi channel EEG and MEG with diminished bias from common sources," *Human Brain Mapping*, vol. 28, no. 11. pp. 1178–1193, 2007.

[92] E. Rodriguez, N. George, J.-P. Lachaux, J. Martinerie, B. Renault, and F. J. Varela, "Perception's shadow: long-distance synchronization of human brain activity," *Nature*, vol. 397, no. 6718. pp. 430–433, 1999.

[93] T. Koenig, D. Studer, D. Hubl, L. Melie, and W. K. Strik, "Brain connectivity at different time-scales measured with EEG," *Philosophical Transactions of the Royal Society B: Biological Sciences*, vol. 360, no. 1457. pp. 1015–1024, 2005.

[94] D. Studer, U. Hoffmann, and T. Koenig, "From EEG dependency multichannel matching pursuit to sparse topographic EEG decomposition," *Journal of Neuroscience Methods*, vol. 153, no. 2. pp. 261–275, 2006.

[95] S. Aviyente, E. M. Bernat, W. S. Evans, and S. R. Sponheim, "A phase synchrony measure for quantifying dynamic functional integration in the brain," *Human Brain Mapping*, vol. 32, no. 1. pp. 80–93, 2011.

Research Highlight:

- Quasi-stable phase synchronized patterns are observed in β band of multichannel EEG
- Synchrostates characterize the temporal brain dynamics found during face perception
- Inter-synchrostate transitions are semi-deterministic and depends on the stimulus
- Phase synchronization index for EEG synchrostates yields functional brain networks
- Complex network measures can be used to understand information processing in brain